Mating activates neuroendocrine pathways signaling hunger in *Drosophila* females

Meghan Laturney[^], Gabriella R. Sterne, and Kristin Scott[^,#]

University of California, Berkeley, United States;

[^]Corresponding authors: meghan.laturney@berkeley.edu, kscott@berkeley.edu

[#] Lead contact

Summary

Mated females reallocate resources to offspring production, causing changes in nutritional requirements and challenges to energy homeostasis. Although observed in most species, the neural and endocrine mechanisms that regulate the nutritional needs of mated females are not well understood. Here, we investigate the neural circuitry that regulates sugar appetite in mated *Drosophila melanogaster* females. During copulation, a male-derived sex peptide is transferred to females, silencing the mating status circuit to elicit many postmating behavioral changes[1-3]. We find that increased sucrose consumption is a postmated female behavior and show that it is mediated by the mating status circuit. We discovered that sexually dimorphic insulin receptor (Lgr3) neurons integrate mating status and nutritional state signals to adjust sucrose consumption. Lgr3+ cells receive inhibitory input from the mating status circuit via female specific pCd-2 neurons. In mated females, the inhibition of Lgr3 cells from pCd-2 is attenuated, transforming the mated signal into a long-term hunger signal that promotes sugar intake. Our results thus demonstrate that the mating circuit alters nutrient sensing centers in

23 females to promote sugar consumption, providing a mechanism to increase intake in
24 anticipation of the energetic costs associated with reproduction.

25 **Main**

26 Female mating status impacts feeding decisions across species. In *Drosophila*, mated
27 females increase total food intake[4] and develop specific appetites for protein and salt[5-7]. Sugar,
28 another macronutrient, is vitally important for flies and is their main energy source[8]. In mated
29 females, increased activity[9] results in elevated metabolic rates[10] driving the need for additional
30 calories. Moreover, females pack eggs with lipids[11] synthesized from dietary carbohydrates[10].
31 Together, this predicts that mated females require significantly more sugar than virgins.
32 However, as excessive sugar negatively impacts fly health[12], sugar intake must be tightly
33 regulated. Although the sugar to protein ratio influences reproductive output and longevity[8], the
34 absolute levels of sugar intake of mated females remain untested.

35 In *Drosophila*, mated related changes in females are orchestrated by sex peptide (SP), a
36 36-amino acid peptide that is produced in the male seminal fluid and transferred to females
37 during copulation[1,2]. SP binds to its receptor (SPR)[13] which is expressed in sensory neurons
38 (SPSNs) in the uterus[14,15]. SPSNs convey mating status to sex peptide abdominal ganglia (SAG)
39 neurons that ascend to the central brain[3] and synapse onto pC1 neurons[16]. This female-specific
40 SPSN-SAG-pC1 circuit is active in virgin females and silenced after mating[3,16]. Reception of SP
41 and silencing of this circuit initiates the long-term postmating response in females, which
42 includes changes in egg laying and sexual receptivity[3,16,17]. The second-order SAG neurons also
43 drive changes in salt and protein appetites[7], demonstrating that the mating status circuit alters
44 food consumption in mated females. However, how the mating circuit influences nutritional state
45 circuits or feeding circuits remains a central question. Here, we use automated behavioral assays

46 for measuring consumption, powerful genetic tools, connectomics, and functional imaging
47 approaches to examine neural mechanisms for appetite changes in mated females.
48 To investigate the impact of female mating status on sugar intake, we monitored
49 individual feeding bouts over time using a high-throughput, automated feeding platform (FLIC[18],
50 Fig. 1a). We compared consumption of virgins and two types of mated females (1-hr or 72-hr
51 postmated). We found that 72-hr postmated females consumed for a significantly longer duration
52 on sucrose solution than virgins or 1-hr postmated females (Fig. 1b). To further evaluate the
53 onset of increased sucrose consumption, we monitored consumption of virgin, 24-hr postmated
54 females, and 72-hr psotmated females and established a postmated phenotype in both mated
55 groups (Fig. 1c). These studies demonstrate that mated females consume more sugar than virgins
56 and that changes in sucrose consumption manifest 6-24hr after copulation.
57 To explore differences in feeding dynamics, virgin and mated females were allowed to
58 feed on different sucrose concentrations and the number and length of feeding bouts were
59 examined. Mated females consumed for longer durations than virgins for all sucrose
60 concentrations below 500mM (Fig. 1d). Investigation into the microstructure of feeding revealed
61 that the postmated increase in sucrose consumption is due to an elongation in feeding bout
62 duration rather than an increased number of bouts (Fig. 1e,f). Thus, like hungry flies[19], mated
63 females consume more by engaging in longer feeding times rather than by initiating more
64 feeding events.
65 We tested two predictions suggested by the mating-induced changes in sugar feeding
66 dynamics. First, longer overall feeding durations suggest that a greater amount of sugar is
67 consumed. We directly tested this using a capillary feeder (CAFE[20], Fig. 1g) and found that
68 mated females consume significantly more sucrose than virgins (Fig. 1h). Second, virgin and

69 mated females execute a similar number of feeding bouts, suggesting that females do not differ
70 in the probability of initiating a feeding event. To directly test this, we monitored proboscis
71 extension upon sugar taste detection (Fig. 1i) and found that virgin and mated females have
72 similar feeding initiation propensities (Fig. 1j,k). These results further corroborate that increased
73 sugar consumption in mated females is due to longer meal duration rather than more frequent
74 feeding bouts.

75 Hunger increases the sensitivity of gustatory neurons to sugar[21]. To test whether changes
76 in sugar sensory sensitivity underlie increased sucrose consumption in mated females, we
77 monitored taste-induced neural activity in sugar gustatory neurons in mated and virgin females
78 with the GCaMP6s calcium indicator (Fig. 1l). Stimulation of the fly proboscis with sugar
79 elicited similar responses in gustatory axons regardless of mating status (Fig. 1m-o),
80 demonstrating that gustatory sensitivity is not altered by mating and not likely to contribute to
81 changes in feeding.

82 As mating increases egg production, we reasoned that the increase in sucrose
83 consumption could be driven by a need-dependent mechanism. In this scenario, mating induces
84 egg production, depleting energy stores and driving a need for sucrose consumption to restore
85 homeostasis. To test this, we quantified sucrose consumption of virgin and mated eggless
86 females with both FLIC and CAFE (Fig. 2a and Extended Data Fig.1a, respectively). We found
87 that despite a lack of egg production[7,22,23], mated females consumed more sucrose than virgins,
88 demonstrating that the change in postmated sucrose feeding is not driven by egg production
89 itself. Instead, this result suggests that sucrose feeding changes are anticipatory in nature and a
90 consequence of a need-independent mechanism.

91 Postmated changes in female behavior are elicited by sex peptide (SP)[1,2,24], a male-
92 derived seminal fluid peptide and require female uterine primary sensory neurons (SPSNs)[13-15]
93 (Fig. 2b). To test the involvement of the SPSNs in postmated sucrose feeding changes, we
94 genetically accessed SPSNs using three different genetic driver combinations (see methods). All
95 genetic intersections consistently labeled at least 4 SPSNs (Fig. 2c, Extended Data Fig.1b,c) with
96 no overlap of off-target neurons (Extended Data 1d), making them useful tools to investigate the
97 role of the SPSNs in postmating feeding changes. We silenced the SPSNs in virgin females using
98 constitutive silencers (either the potassium inward rectifier, KIR2.1, or the tetanus toxin light
99 chain, TNT) to mimic the mated state and measured sucrose consumption. Virgin females with
100 SPSNs silenced consumed significantly more sucrose than virgin controls (Fig. 2d, Extended
101 data 1e,f), recapitulating the mated phenotype. This data argues that mated females increase
102 sucrose consumption after mating via the SPSNs.
103 The canonical sex peptide pathway for postmated changes in female behavior is a three-
104 layer circuit from SPSNs to SAGs to pC1[3,16,17]. As with the SPSNs, SAG and pC1 neurons are
105 active in a virgin female and silenced in a mated female[3,16]. To precisely manipulate SAGs, we
106 generated a new split-GAL4 line (SAG-SS3, Fig. 2m). Next, we acutely silenced SAGs by
107 driving the expression of the green-light gated anion channelrhodopsin (GtACR1) with SAG-
108 SS3. Monitoring consumption over time, we found that acutely silencing SAGs significantly
109 increased sucrose consumption (Fig. 2n, Extended Data Fig. 2a). Although an off-target
110 ascending neuron is also labeled in SAG-SS3, it is not responsible for changes in sucrose
111 consumption (Extended Data Fig. 3), arguing that the increased sucrose consumption observed
112 with SAG-SS3 is due to the activity of SAG neuron itself. Downstream of SAG, we found that
113 acutely silencing pC1 also significantly increased sucrose consumption (Fig. 2o,p, Extended

114 Data Fig. 2b-d), demonstrating that pC1 neurons regulate postmating sucrose feeding. Taken
115 together, we conclude that the increased sugar consumption after mating is part of the repertoire
116 of behavioral changes induced after copulation by sex peptide acting on the SPSN-SAG-pC1
117 mating status circuit.

118 Postsynaptic to pC1, the mating status circuit splits into separate neural pathways that
119 mediate different behavioral subprograms, including circuits that elicit changes in sexual
120 receptivity[17] or egg-laying[16]. We hypothesized that the neural circuit supporting the postmated
121 increase in sucrose consumption could either follow one of the established circuits or diverge
122 after pC1. To test if sucrose feeding is executed by previously identified postmating subcircuits,
123 we optogenetically manipulated the activity of the descending neurons (DNs) for sexual
124 receptivity (vpoDNs) or egg laying (oviDNs) to mimic the mated state (Fig. 3a) and measured
125 sucrose consumption. We found no difference in sucrose consumption upon manipulation of
126 vpoDNs or oviDNs (Fig. 3b,c,f,g, Extended Data Fig. 2e-h). We note that we measured sucrose
127 intake in immobilized flies for oviDN manipulations, as activating oviDNs caused females to
128 stop walking (Fig. 3d,e), likely a natural component of egg laying. These studies argue that
129 neither of the previously identified circuits responsible for a single postmating response, egg
130 laying and sexual receptivity, mediate postmating sucrose feeding.

131 To identify novel pathways that mediate changes in mated feeding behavior, we
132 examined other major outputs of the mating status circuit. We identified postsynaptic partners of
133 SAG and pC1 using automated analysis[25,26] of a fly brain electron microscopy (EM)
134 connectome[27,28]. This approach identified three pCd-2 neurons[29,30], pCd-2a, pCd-2b, and pCd-2c
135 (Fig. 4a, Extended Data Fig. 4a), that are strongly connected to SAG (39 synapses) and pC1 (158
136 synapses). These neurons are promising candidates to mediate postmating feeding changes

137 because their processes descend into the prow region of the Subesophageal Zone (SEZ, Fig.
138 4b,c), a brain region implicated in energy homeostasis and feeding[31]. As pC1 and SAG are
139 cholinergic[3,16], pCd-2 cells likely receive excitatory signals from these two upstream synaptic
140 partners and therefore would be predicted to be less active in mated females (Fig. 4d). We
141 generated split-GAL4 lines to genetically access pCd-2a and pCd-2b (Fig. 4e,f) and found that
142 both neurons are female-specific (Extended Data Fig. 4b), consistent with a role in female
143 postmating behavior. Optogenetically silencing either pCd-2a or pCd-2b significantly increased
144 sucrose consumption, recapitulating the mated state (Fig. 4h,I, Extended Data Fig. 5c-j).
145 Importantly, silencing pCd-2a or pCd-2b did not influence egg laying (Fig. 4g, Extended Data
146 Fig. 5a,b), demonstrating separation of circuits for increased sucrose consumption from other
147 behaviors downstream of pC1.

148 To examine how pC1 influences sucrose consumption, we used EM analyses and
149 identified the major downstream targets of pCd-2 as t-shaped cells (711 synapses) having
150 processes in the SEZ prow region and a neuroendocrine center, the pars intercerebralis, with
151 terminal arbors similar to insulin producing cells and other median secretory cells[32] (Fig. 5a,
152 Extended Data Fig. 6). Based on anatomical similarity, these cells are Lgr3+ (leucine-rich repeat
153 G-protein-coupled receptor[33]) medial bundle neurons (mBNs) (Fig. 5b,c). Lgr3 expression is
154 sexually dimorphic, found specifically in the central brain and abdominal ganglia of females[34],
155 consistent with a role in female behavior. Moreover, Lgr3 is a receptor for the *Drosophila*
156 insulin-like peptide 8 (Dilp8[35-37]), and both Lgr3 and Dilp8 are known to regulate feeding[38].
157 These findings suggest that the Lgr3+ mBNs may represent the site where mating status circuits
158 interact with hunger/satiety circuits to regulate feeding.

159 To test this hypothesis, we first examined whether Lgr3+ mBNs are functionally
160 connected to pC1, pCd-2a, or pCd-2b by optogenetically activating these populations while
161 simultaneously measuring calcium responses in Lgr3+ neurons. In all cases, neural activation
162 caused significant calcium decreases in Lgr3+ neurons (Fig. 5d-f), validating Lgr3+ mBNs as
163 targets of the mating status pathway. As pC1 is inhibited in the mated state, our studies argue
164 that Lgr3+ mBNs are more active in mated females (Fig. 5g). To examine whether activity in
165 Lgr3+ mBNs influences consumption, we targeted this population with a genetic intersectional
166 approach (R19B09∩fru[34], Fig. 5c), optogenetically activated Lgr3+ mBNs, and monitored
167 sucrose consumption. We found that increased activity in Lgr3+ mBNs promotes sucrose
168 consumption, mimicking the mated state (Fig. 5h). Together, these studies reveal that Lgr3+
169 mBNs receive inputs from the canonical postmating pathway and are part of a neuroendocrine
170 pathway that regulates sucrose consumption in postmated females.
171 In conclusion, we report a new postmated response of increased sucrose consumption,
172 which independent of caloric deficiencies caused by egg production and anticipatory in
173 nature. Our findings provide a neural mechanism for the coordination of mating state and
174 sucrose consumption (Fig. 5g). In virgins, increased activity of SAG and pC1 potentiates pCd-2-
175 mediated inhibition of Lgr3+ cells within the endocrine center of the brain, resulting in low sugar
176 intake. After mating, the activity of SAG and pC1 is reduced[3,16], decreasing the activity of pCd-2
177 and alleviating the inhibition from *Lgr3*+ cells, increasing sucrose intake.
178 The sexually dimorphic Lgr3+ neurons are the nexus integrating mating status and
179 neuroendocrine hunger signaling. Lgr3 is a leucine-rich repeat containing G-protein coupled
180 receptor, which binds Dilp8 to regulate feeding in flies. Expression levels of Lgr3 and Dilp8 rise
181 in fed flies and mutations in either gene increase feeding, arguing that Dilp8 and Lgr3 are satiety

182 factors[38]. Our calcium imaging and behavioral studies of Lgr3+ mBNs indicate that they are
183 more active in a mated state and promote sucrose consumption. Together, these data suggest a
184 model for how Lgr3+ mBN neurons integrate signals from the mating status and hunger/satiety
185 systems. In virgin or satiated female flies, circulating DILP8 and pCd-2 activity, respectively,
186 inhibit Lgr3+ mBNs (Fig. 5g), reducing sugar feeding. Conversely, in mated or hungry flies,
187 Lgr3+ mBNs lack the inhibitory signal from pCd-2 neurons or circulating Dilp8, respectively,
188 resulting in increased sugar consumption. Hence, the mated state may be viewed mechanistically
189 as an additional "hunger" signal within this system.

190 Thus, we report that an elevated appetite for sucrose is an important behavioral
191 subprogram elicited by mating and executed by female-specific circuitry, shifting the physiology
192 of a mated female. The activation of hunger centers by the mating status circuit provides a neural
193 mechanism that anticipates the large energetic demands associated with offspring production and
194 increases caloric intake, promoting reproductive success.

195 **References**
196

197 1. Chen, P. S., Stumm-Zollinger, E., Aigaki, T., Balmer, J., Bienz, M. & Böhlen, P. A male
198 accessory gland peptide that regulates reproductive behavior of female D. melanogaster.
199 *Cell***54**, 291-298 (1988).
200 2. Liu, H. & Kubli, E. Sex-peptide is the molecular basis of the sperm effect in Drosophila
201 melanogaster. *Proc. Natl. Acad. Sci. USA***100**, 9929-9933 (2003).
202 3. Feng, K., Palfreyman, M. T., Häsemeyer, M., Talsma, A. & Dickson, B. J. Ascending
203 SAG neurons control sexual receptivity of Drosophila females. *Neuron***83**, 135-148
204 (2014).
205 4. Carvalho, G. B., Kapahi, P., Anderson, D. J. & Benzer, S. Allocrine modulation of
206 feeding behavior by the sex peptide of Drosophila. *Curr. Biol.* **16**, 692-696 (2006).
207 5. Vargas, M. A., Luo, N., Yamaguchi, A. & Kapahi, P. A role for S6 kinase and serotonin
208 in postmating dietary switch and balance of nutrients in D. melanogaster. *Curr. Biol*. **20**,
209 1006-1011 (2010).
210 6. Ribeiro, C. & Dickson, B. J. Sex peptide receptor and neuronal TOR/S6K signaling
211 modulate nutrient balancing in Drosophila. *Curr. Biol*. **20**, 1000-1005 (2010).
212 7. Walker, S. J., Corrales-Carvajal, V. M. & Ribeiro, C. Postmating circuitry modulates salt
213 taste processing to increase reproductive output in Drosophila. *Curr. Biol*. **25**, 2621-2630
214 (2015).

8. Simpson, S. J., Le Couteur, D. G. & Raubenheimer, D. Putting the balance back in diet. *Cell***161**, 18-23 (2015).
9. Isaac, R. E., Li, C., Leedale, A. E. & Shirras, A. D. Drosophila male sex peptide inhibits siesta sleep and promotes locomotor activity in the post-mated female. *Proc. Biol. Sci.* **277**, 65-70 (2010).
10. Brown, E. B., Klok, J. & Keene, A. C. Measuring metabolic rate in single flies during sleep and waking states via indirect calorimetry. *J. Neurosci. Methods***376**, doi: 10.1016/j.jneumeth.2022.109606 (2022).
11. Sieber, M. H & Spradling, A. C. Steroid signaling establishes a female metabolic state and regulates SREBP to control ooctyte lipid accumulation. *Curr. Biol*. **25**, 993-1004 (2015).
12. Baenas, N. & Wagner, A. E. Drosophila melanogaster as a model organism for obesity and type-2 diabetes mellitus by applying high-sugar and high-fat diets. *Biomolecules***12**, doi: 10.3390/biom12020307 (2022).
13. Yapici, N., Kim, Y. J., Ribeiro, C. & Dickson, B. J. A receptor that mediates the post-mating switch in Drosophila melanogaster reproductive behavior. *Nature***451**, 33-37 (2008).
14. Häsemeyer, M., Yapici, N., Heberlein, U. & Dickson, B. J. Sensory neurons in the Drosophila genital tract regulate female reproductive behavior. *Neuron***61**,511-518 (2009).
15. Yang, C. H., Rumpf, S., Xiang, Y., Gordon, M. D., Song, W., Jan, L. Y. & Jan, Y. N. Control of the postmating behavioral switch in Drosophila females be internal sensory neurons. *Neuron***61**, 519-526 (2009).
16. Wang, F., Wang, K., Forknall, N., Patrick, C., Yang, T., Parekh, R., Bock, D. & Dickson, B. J. Neural circuitry linking mating and egg laying in Drosophila females. *Nature***579**, 101-105 (2020).
17. Wang, K., Wang, F., Forknall, N., Yang, T., Patrick, C., Parekh, R. & Dickson, B. J. Neural circuit mechanisms of sexual receptivity in Drosophila females. *Nature***589**, 577-581 (2021).
18. Ro, J., Harvanek, Z. M. & Pletcher, S. D. FLIC: high-throughput, continuous analysis of feeding behaviors in Drosophila. *PLoS One***9**, doi: 10.1371/journal.pone.0101107 (2014).
19. Itskov, P., Moreira, J. M., Vinnik, E., Lopes, G., Safarik, S, Dickinson, M. H. & Ribeiro, C. Automated monitoring and quantitative analysis of feeding behaviour in Drosophila. *Nat. Commun*. **5**, doi: 10.1038/ncomms5560 (2014).
20. Ja, W. W., Carvalho, G. B., Mak, E. M., de la Rosa, N. N., Fang, A. Y., Liong, J. C., Brummel, T. & Benzer, S. Prandiology of Drosophila and the CAFE assay. *Proc. Natl. Acad. Sci. USA***104**, 8253-8256 (2007).
21. Inagaki, H. K., Panse, K. M. & Anderson, D. J. Independent, reciprocal neuromodulatory control of sweet and bitter taste sensitivity during starvation in Drosophila. *Neuron***84**, 806-820 (2014).
22. Ohlstein, B. & McKearin, D. Ectopic expression of the Drosophila Bam protein eliminates oogenic germline stem cells. *Development***124**, 3651-3662 (1997).
23. Mével-Ninio, M., Fouilloux, E., Guénal, I & Vincent, A. The three dominant female-sterile mutations of the Drosophila ovo gene are point mutations that create new translation-initiator AUG codons. *Development***122**, 4131-4138 (1996).

24. Laturney, M. & Billeter, J. C. Neurogenetics of female reproductive behaviors in Drosophila melanogaster. *Adv. Genet*. **85**, 1-108 (2015).
25. Buhmann, J. et al. Automatic detection of synaptic partners in a whole-brain Drosophila electron microscopy data set. *Nat. Methods***7**, 771-774 (2021).
26. Heinrich, L., Funke, J., Pape, C., Nunez-Iglesias, J. & Saalfeld, S. Synaptic cleft segmentation in non-isotropic volume electron microscopy of the complete Drosophila brain. arXiv:180502718 [csCV]. (2018).
27. Zheng, Z. et al. A complete electron microscopy volume of the brain of adult Drosophila melanogaster. *Cell***174**, 730-743 (2018).
28. Dorkenwald, S. et al. FlyWire: online community for whole-brain connectomics. *Nat. Methods***1**, 119-128 (2022).
29. Kimura, K., Sato, C., Koganezawa, M. & Yamamoto, D. Drosophila ovipositor extension in mating behavior and egg deposition involves distinct sets of brain interneurons. *PLoS ONE***10**, e0126445 (2015).
30. Nojima, T., Rings, A., Allen, A. M., Otto, N., Verschut, T. A., Billeter, J. C., Neville, M. C. & Goodwin, S. F. A sex-specific switch between visual and olfactory inputs underlies adaptive sex differences in behavior. *Curr. Biol*. **31**, 1175-1192 (2021).
31. Shiu, P. K., Sterne, G. R., Engert, S., Dickson, B. J. & Scott, K. Taste quality and hunger interactions in a feeding sensorimotor circuit. *Elife***11**, doi: 10.7554/eLife.79887 (2022).
32. Liao, S. & Nässel, D. R. Drosophila insulin-like peptide 8 (DILP8)in ovarian follicle cells regulates ovulation and metabolism. *Front. Endocrinol.* **11**, doi: 10.3389/fendo.2020.00461 (2020).
33. Dolan. J. et al. The extracellular leucine-rich repeat superfamily; a comparative survey and analysis of evolutionary relationships and expression patterns. *BMC Genomic***8**, doi: 10.1186/1471-2164-8-320 (2007).
34. Meissner, G. W., Luo, S. D., Dias, B. G., Texada, M. J. & Baker, B. S. Sex-specific regulation of Lgr3 in Drosophila neurons. *Proc. Natl. Acad. Sci. USA***113**, 1256-1265 (2016).
35. Colombani, J., Andersen, D. S., Boulan, L., Boone, E., Romero, N., Virolle, V., Texada, M. & Léopold, P. Drosophila Lgr3 couples organ growth with maturation and ensures developmental stability. *Curr. Biol.* **25**, 2723-2729 (2015).
36. Garelli, A. et al. Dilp8 requires the neuronal relaxin receptor Lgr3 to couple growth to developmental timing. *Nat. Commun*. **6**, doi: 10.1038/ncomms9732 (2015).
37. Vallejo, D. M., Juarez-Carreño, S., Bolivar, J., Morante, J. & Dominguez, M. A brain circuit that synchronizes growth and maturation revealed through Dilp8 binding to Lgr3. *Science***350**, doi: 10.1126/science.aac6767 (2015).
38. Yeom, E. et al. Tumour-derived Dlip8/INSL3 induces cancer anorexia by regulating feeding neuropeptides via Lgr3/8 in the brain. *Nat. Cell Biol.* **23**, 172-183 (2021).

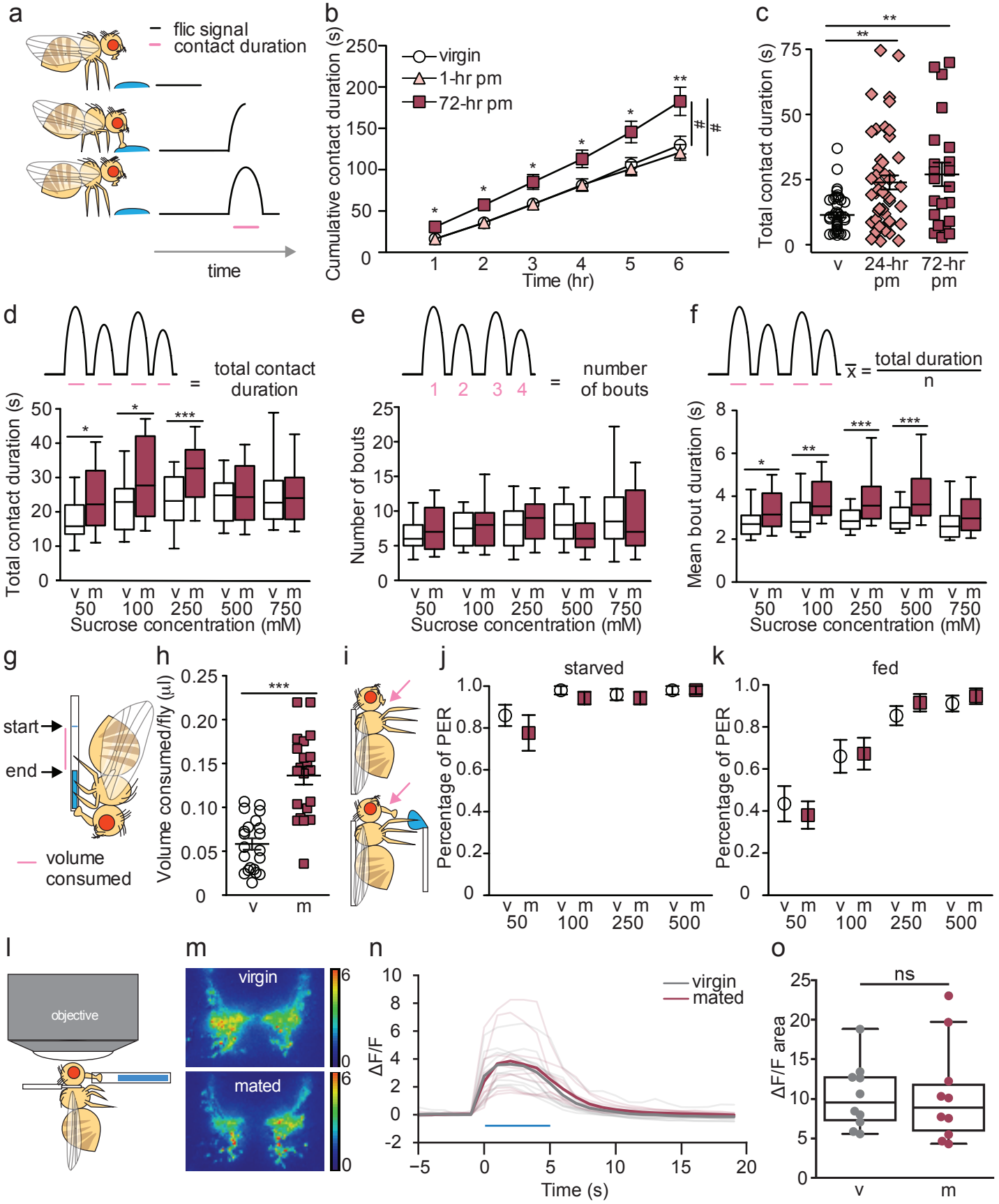
a
flic signal
contact duration
time
b
virgin
1-hr pm
72-hr pm
Cumulative contact duration (s)
Time (hr)
c
Total contact duration (s)
v
24-hr pm
72-hr pm
d
= total contact duration
Total contact duration (s)
Sucrose concentration (mM)
e
1 2 3 4
= number of bouts
Number of bouts
Sucrose concentration (mM)
f
x̄ = total duration / n
Mean bout duration (s)
Sucrose concentration (mM)
g
start
end
volume consumed
h
Volume consumed/fly (µl)
i
j
starved
Percentage of PER
k
fed
Percentage of PER
l
objective
m
virgin
mated
n
virgin
mated
ΔF/F
Time (s)
o
ΔF/F area
ns

Fig. 1. Mated females consume more sucrose than virgins by elongating feeding events.

a, Schematic of fly feeding behavior (left) and the FLIC signal that monitors food contact over time (right). **b**, Cumulative drinking time in FLIC of virgin (white circles, n=34), 1-hr postmated (pm) (light pink triangles, n=30), and 72-hr pm (dark pink squares, n=28) females. Line graph shows mean and s.e.m. over time. Kruskal-Wallis was used to compare groups at hour intervals, Dunn's posthoc. **c**, Total drinking time in FLIC in 20-min assay of virgin (v; n=47), 24-hr pm (n=47), and 72-hr pm (n=22) females, Kruskal-Wallis, Dunn's posthoc. **d**-**f**, Schematic and plots of feeding behavior of virgin (v) and mated (m) females presented with sucrose of varying concentrations in FLIC 20-min assay (n=33-36) examining total drinking time (**d**), number of drinking bouts (**e**), and average bout duration (**f**). Box plot show first to third quartile, whiskers span 10-90 percentile, Mann Whitney. **g**, Schematic of female drinking from capillary containing sucrose solution in CAFE assay. **h**, Total volume consumed in CAFE assay per fly in 24 hours by virgin (v, n=21) and mated females (m, n=21), unpaired t-test. **i**, Schematic of proboscis extension response (PER) assay. **j**-**k**, Percentage of proboscis extensions observed per fly upon three presentations of sucrose of indicated concentration in virgin (v) and mated (m) females in starved (n=17-18, **j**) and fed state (n=16, **k**), Mann Whitney. **l**, Schematic of in vivo calcium imaging experiment monitoring taste-induced activity in gustatory axons. **m**-**o**, Changes in GCaMP6s signal in virgin (grey) and mated (dark pink) females, shown as representative fluorescent changes in single brains (**m**), changes over time (**n**), and maximum changes (**o**), n=10. Blue bar represents proboscis sucrose stimulation, Wilcoxen Rank test. *$p<0.05$, **$p<0.01$, ***$p<0.001$, ns = not significant. Scatter plot show mean +/- s.e.m. (**c**,**h**,**o**). Column graph show mean +/- s.e.m. (**j**,**k**). For full genotypes, see Supplementary Data Table 1.

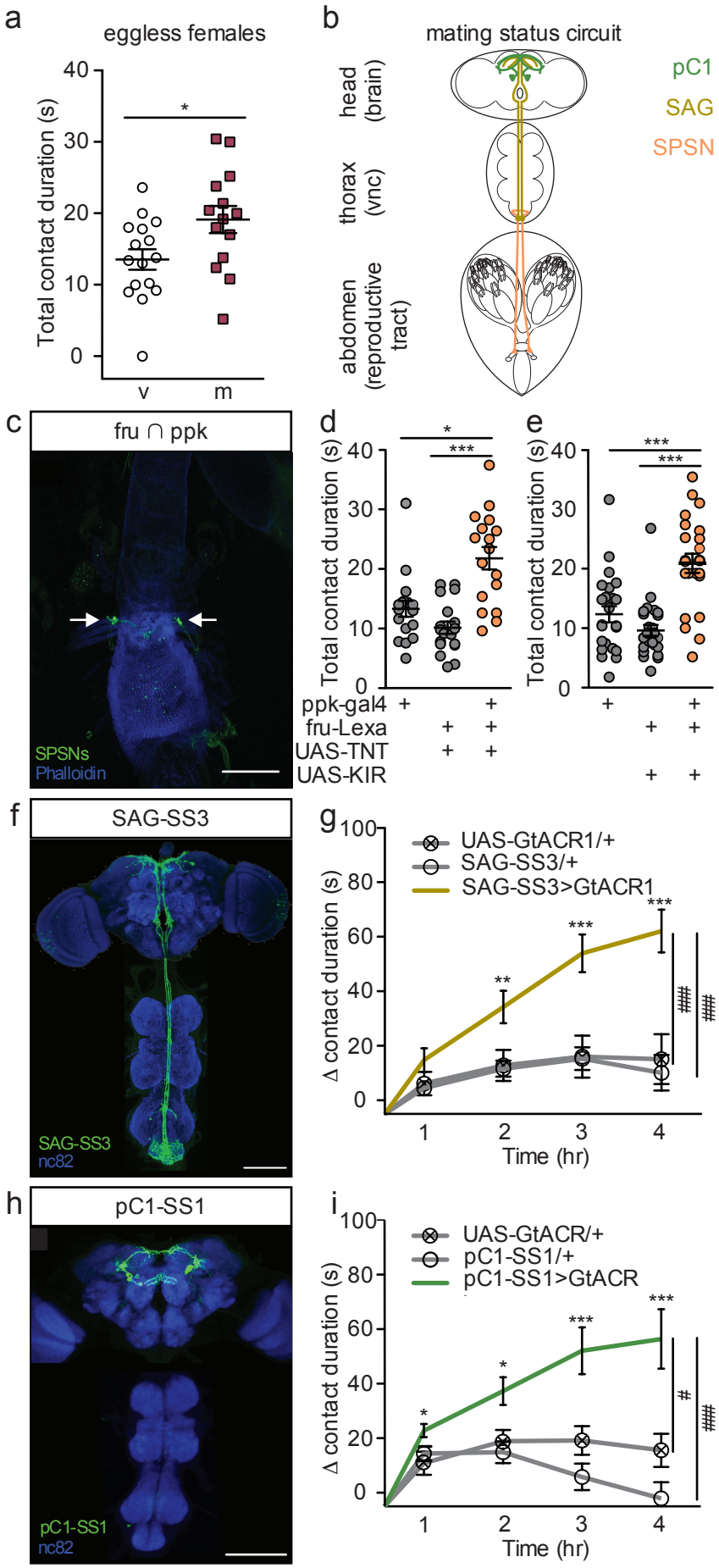

Fig. 2. Postmated increases in sucrose consumption are induced by the canonical mating status circuit and are independent of egg-production.

a, Total drinking time in FLIC in 20-min assay of eggless virgin (v, n=16) and mated (m, n=15) females, Mann Whitney. **b**, Schematic of female with the mating circuit, showing first order (SPSN, pink-orange), second order (SAG, dark yellow) and third order (pC1, green) neurons. **c**, Confocal image of uterus stained to reveal SPSNs (UAS-CD8:GFP, green, arrowhead indicating cell bodies) and muscle tissue (phalloidin, blue). **d**-**e**, Total drinking time in FLIC in 20-min assay of virgin females of indicated genotype (n=17-28), Kruskal-Wallis, Dunn's posthoc. **f**,**h** Confocal images of brain (top) and ventral nerve cord (bottom) of SAG-SS3 (**f**) and pC1-SS1 (**h**) females, stained to reveal neural projection pattern (UAS-mVenus, green) and all synapses (nc82, blue). **g**-**i**, Drinking time of females exposed to light normalized to dark controls of indicated genotype in FLIC over 4-hrs (each data point is the drinking time of an individual in the light condition minus the daily average drinking time of all females in dark condition within genotype, n=17-39), Kruskal-Wallis, Dunn's posthoc at hour 4, #p<0.05, ###p<0.001. Line graphs show mean and s.e.m. over time. *p<0.05, **p<0.01, ***p<0.001 (**a**,**d**,**e**,**g**,**i**). Scatter plot show mean +/- s.e.m. (**a**,**d**,**e**). Scale bar 50 µm (**c**,**f**,**h**). For full genotypes see Supplementary Table 1.

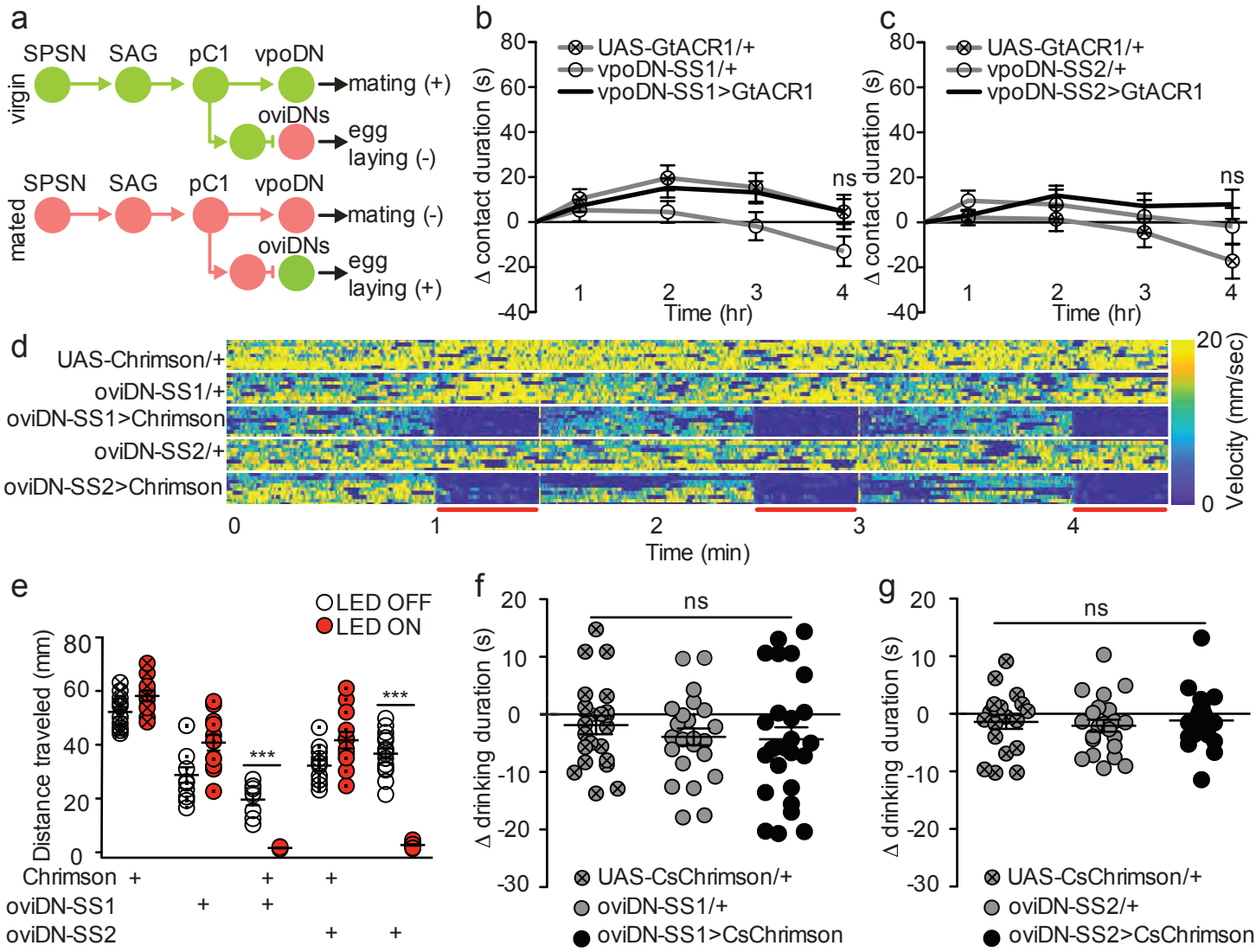

Fig. 3. Descending neurons that regulate egg laying and sexual receptivity do not influence sucrose consumption.

a, Schematic of mating circuit with neural outputs of pC1 and resulting postmating response. Green circles indicate active neurons, salmon circles indicate silenced neurons. **b**-**c**, Difference in drinking time of indicated genotype in FLIC over 4 hrs. Each data point represents normalized drinking time of a single female in light condition (drinking time minus the daily average drinking time of all females in dark condition within genotype, n=20-24), Kruskal-Wallis. Line graph shows mean and s.e.m. over time. **d**, Velocity heatmap upon transient activation in individual walking flies. Red bars indicate light ON (n=8-16). **e**, Total distance traveled in locomotor assay (**d**). ON condition (red) includes 3 30-sec light ON conditions. OFF condition (white) includes 3-30sec light OFF conditions immediately preceding each ON condition, Mann Whitney, ***p<0.001. Aligned dot plot show mean +/- s.e.m. **f**-**g**, Drinking time of females exposed to light normalized to dark controls of indicated genotype in FLIC over 4-hrs (n=19-26), 1way ANOVA, Bonferroni's posthoc. ns = not significant. Scatter plot show mean +/- s.e.m. (**e**-**g**), For full genotypes see Supplementary Data Table 1.

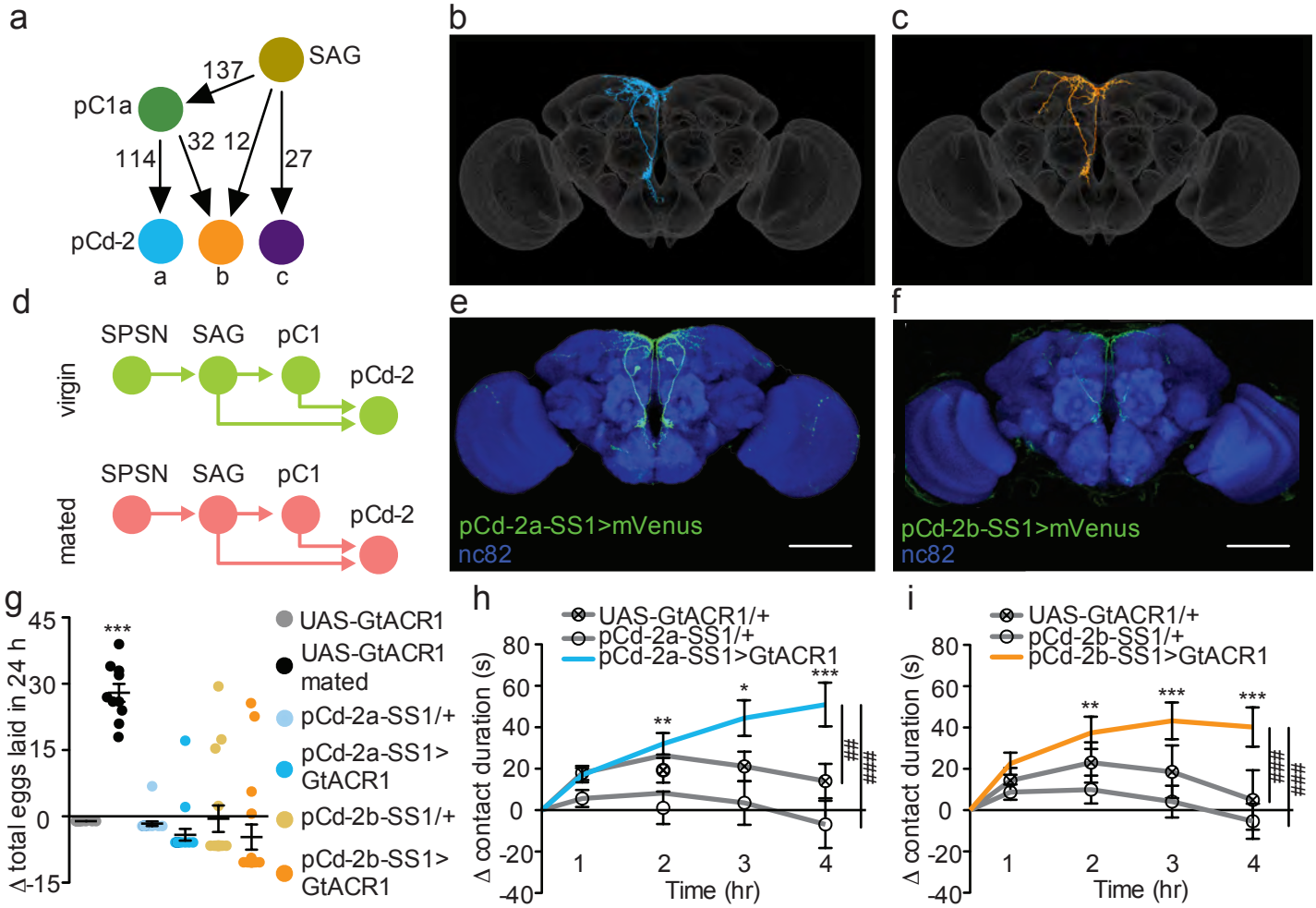

Fig. 4. pCd-2 neural outputs of SAG and pC1 mediate postmating sucrose consumption. **a**, Schematic of neural connectivity of the mating status circuit and pCd-2 cells. Arrows represent direct connection and number indicates number of synapses. **b**-**c**, Electron microscopy reconstruction of pCd-2a,b neurons. **d**, Model of circuit activity in virgin and mated state. Green circles indicate active neurons, salmon circles indicate silenced neurons. **e**-**f**, Confocal images of pCd-2a-SS1 and pCd-2b-SS1 brains, stained to reveal pCd-2 projection pattern (UAS-GFP, green) and all synapses (nc82, blue). Scale bar 50 μm. **g**, Difference in eggs laid in 24-hr of females exposed to light normalized to dark controls (n=10-20). For "UAS-GtACR1 mated" group, data set represents eggs laid by mated females normalized to virgin females of the same genotype. Scatter plot show mean +/- s.e.m., one sample t-test. **h**-**i**, Drinking time of females exposed to light normalized to dark controls of indicated genotype in FLIC over 4-hrs (n=22-26). Line graph show mean and s.e.m. over time, Kruskal-Wallis, Dunn's posthoc at hour 4, ##p<0.01, ###p<0.001. *p<0.05, **p<0.01, ***p<0.001. For full genotypes see Supplementary Table 1.

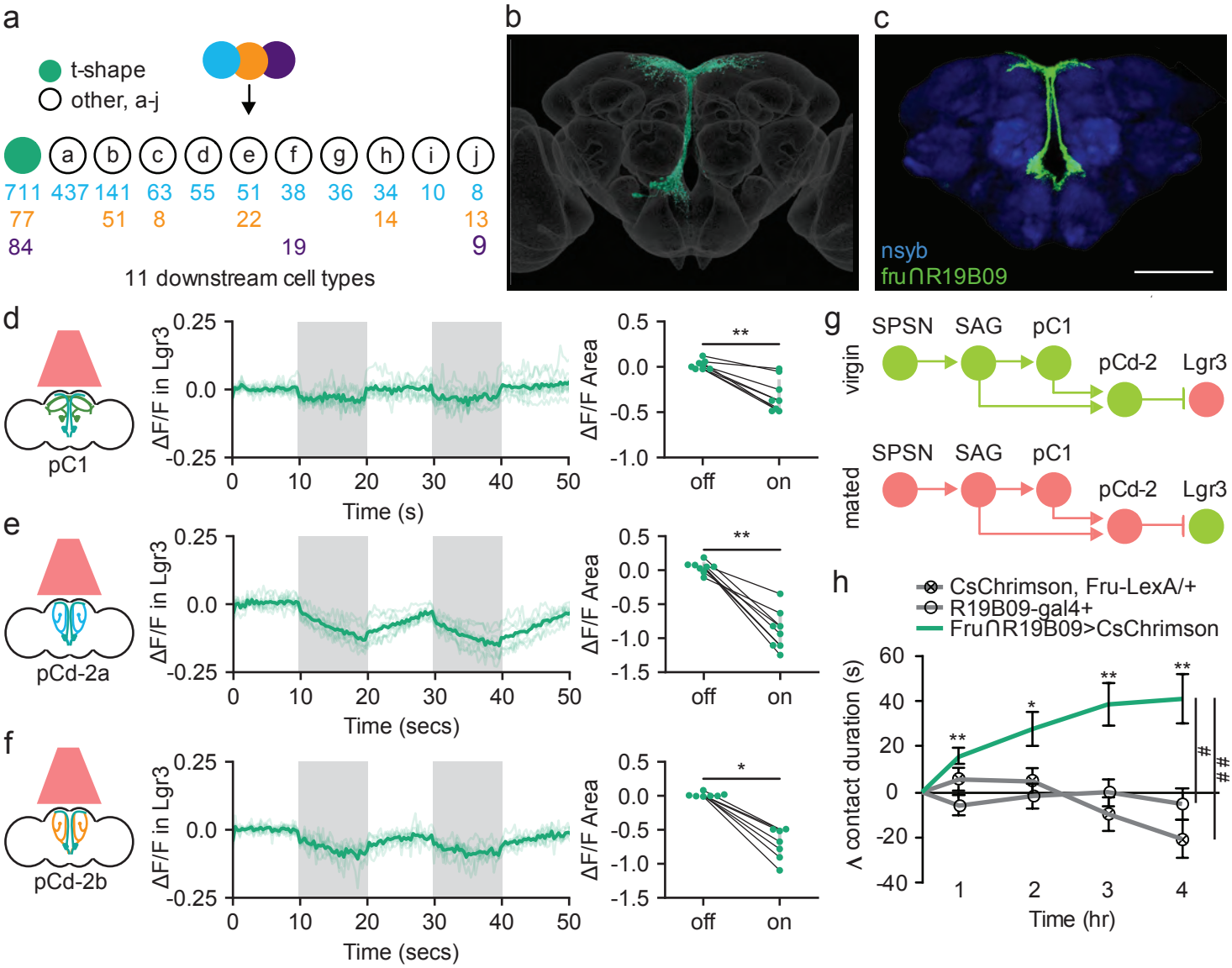

Fig. 5. Sexually dimorphic neuroendocrine Lgr3+ cells receive mating status signals via pCd-2 neurons and regulate sucrose consumption in mated females.

a, Downstream neuronal cell types of pCd-2 cells identified by electron microscopy reconstruction, showing the number of pCd-2 output synapses. T-shape cell type represented with turquoise circles, other cell types represented with white circles (a-j). **b**, Electron microscopy reconstruction of t-shape neurons. **c**, Confocal image of fru+ Lgr3-expressing cells in medial brain (UAS-CD8:GFP, green) and all synapses (nc82, blue). Scale bar 50 µm. **d-f**, Calcium responses of Lgr3-expressing cell bodies in the prow region of the brain to activation of upstream pC1 (**d**), pCd-2a (**e**), or pCd-2b (**f**) neurons (n=7-8) and the analysis of area under the curve, Wilcoxon Rank Test, scatter plot show mean +/- s.e.m. (grey bar). **g**, Neural model for the coordination of mating status and sucrose intake. Green circles indicate active neurons, salmon circles indicate silenced neurons. **h**, Drinking time of females exposed to light normalized to dark controls of indicated genotype in FLIC over 4-hrs (n=10-15). Line graph shows mean and s.e.m. over time, Kruskal-Wallis, Dunn's posthoc at hour 4, #p<0.05, ##p<0.01. *p<0.05, **p<0.01, ***p<0.001. For full genotypes see Supplementary Table 1.

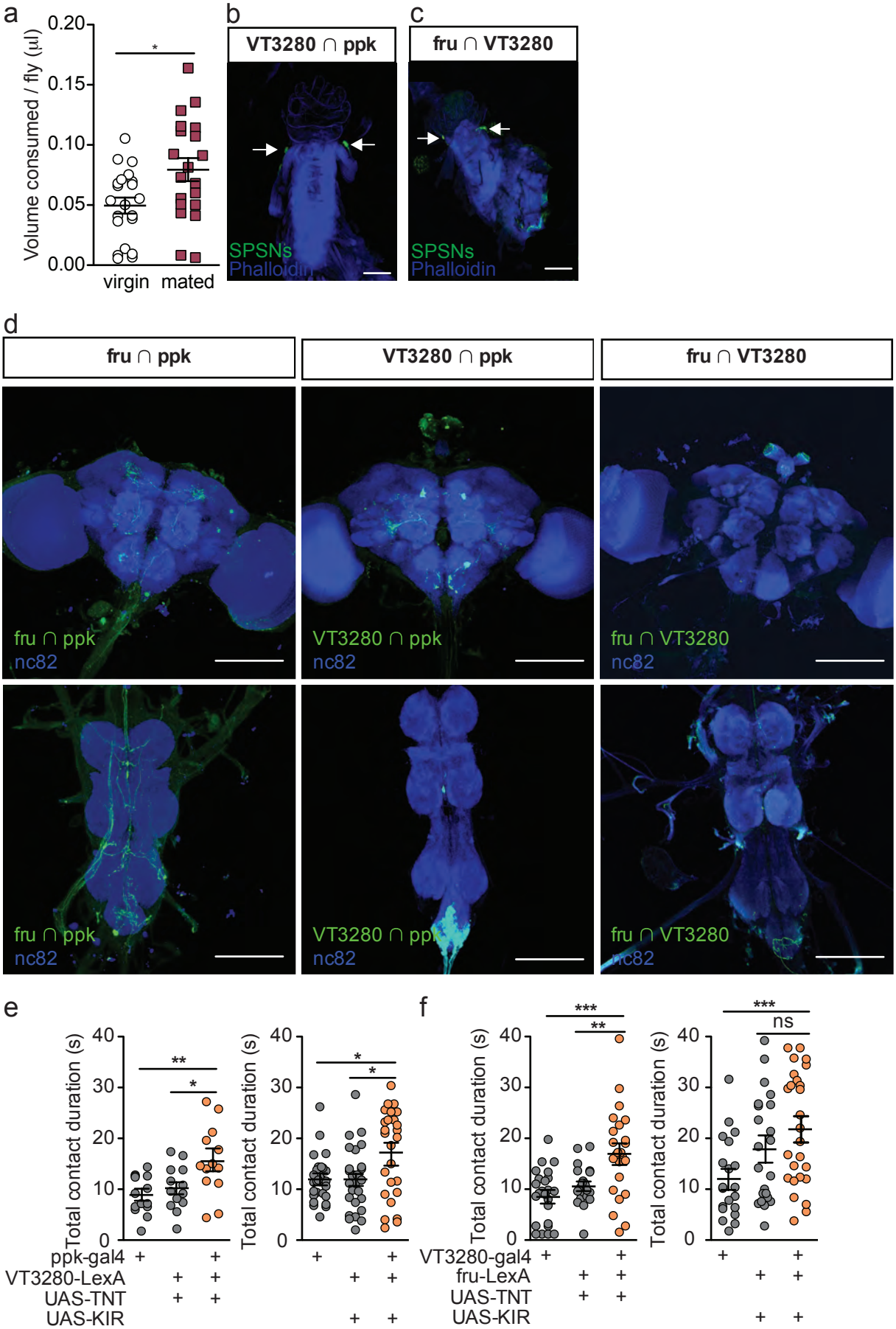
a
Volume consumed / fly (µl)
0.20
0.15
0.10
0.05
0.00
*
virgin
mated
b
VT3280 ∩ ppk
SPSNs
Phalloidin
c
fru ∩ VT3280
SPSNs
Phalloidin
d
fru ∩ ppk
VT3280 ∩ ppk
fru ∩ VT3280
fru ∩ ppk
nc82
VT3280 ∩ ppk
nc82
fru ∩ VT3280
nc82
fru ∩ ppk
nc82
VT3280 ∩ ppk
nc82
fru ∩ VT3280
nc82
e
Total contact duration (s)
40
30
20
10
0
**
*
ppk-gal4
VT3280-LexA
UAS-TNT
UAS-KIR
*
*
f
***
**
***
ns
VT3280-gal4
fru-LexA
UAS-TNT
UAS-KIR

Extended Data Fig. 1. Three independent SPSN lines regulate postmated sucrose consumption.

a, Total volume of 50mM sucrose consumed per fly in CAFE assay by eggless virgin (n=21) and eggless mated females (n=20). *$p<0.05$, unpaired t-test. **b**-**c**, Confocal image of uterus stained to reveal SPSNs (UAS-CD8:GFP, green, arrowhead indicating cell bodies) and muscle tissue (phalloidin, blue). **d**, Confocal images of brain (top) and ventral nerve cord (bottom) of genetic intersections accessing SPSNs stained to reveal off-target neurons in the central nervous system (UAS-GFP; green) and all synapses (nc82; blue). **e**-**f**, Total drinking time in FLIC in 20-min assay of virgin females of indicated genotype (n=19-41). Kruskal-Wallis with Dunn's Multiple Comparison Test revealed differences between silenced females and controls. Scatter plot show mean +/- s.e.m. (**a**,**e**-**f**). Scale bar 50 μm (**b**-**d**).

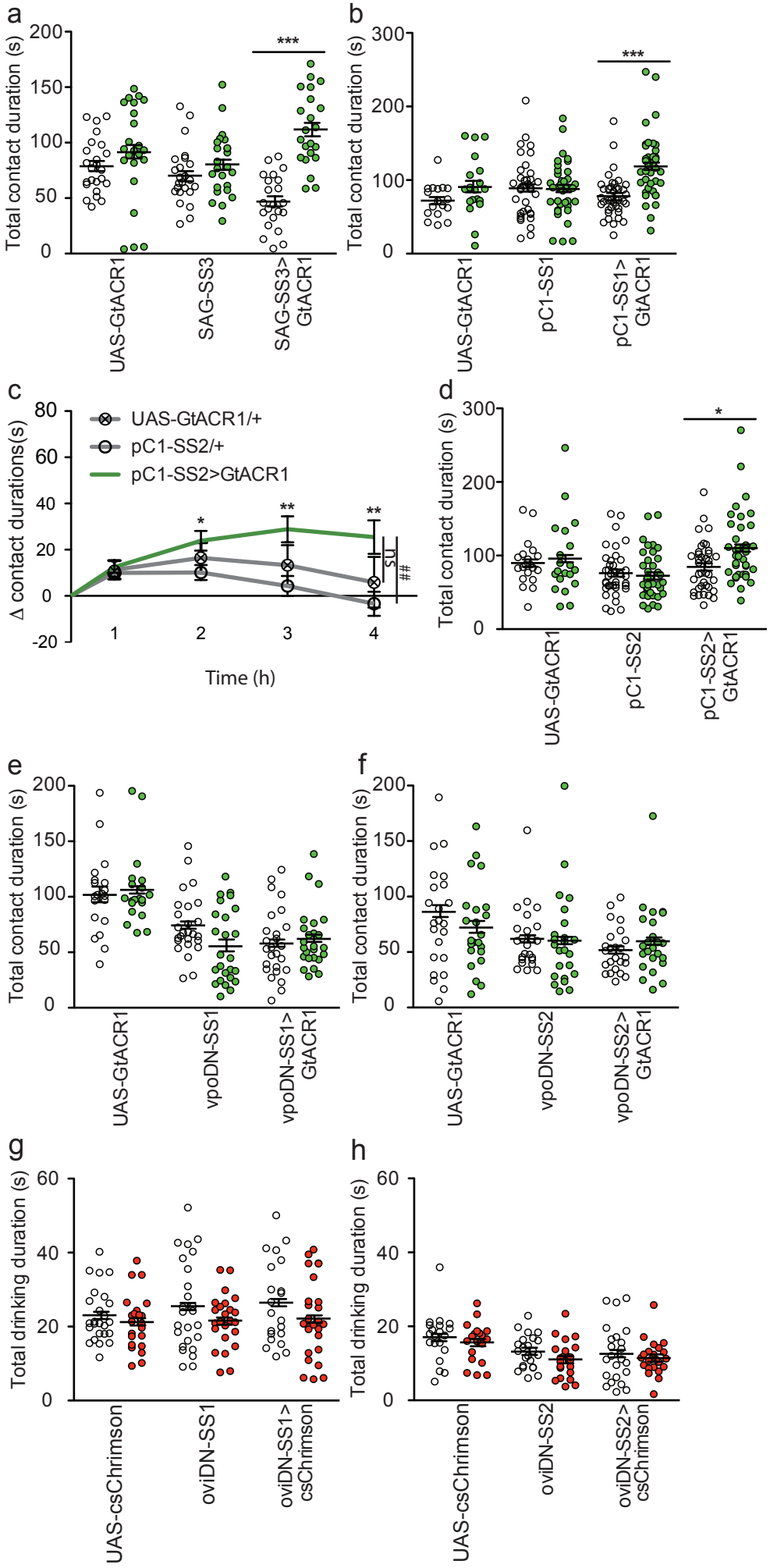

Extended Data Fig. 2.Contact duration times of virgin and mated females upon optogenetic manipulation of neurons in the mating status circuit.

a-b, Total drinking time in FLIC in 4-hr assay of females of indicated genotype and light condition. White circles are dark condition, green circles are green light condition, n=20-32. Data was analyzed with 2way ANOVA and Bonferroni posttests, ***p<0.001. **c**, Drinking time of females exposed to light normalized to dark controls of indicated genotype in FLIC over 4-hrs, n=20-24. Line graphs show mean and s.e.m. over time, Kruskal-Wallis, Dunn's posthoc at hour 4, ##p<0.01, ns = not significant. **d-f**, Total drinking time in FLIC in 4-hr assay of females of indicated genotype and light condition. White circles are dark condition, green circles are green light condition, n=20-32, 2way ANOVA and Bonferroni posttests. **g-h**, Total drinking time in TCA of females of indicated genotype and light condition. White circles are dark condition, red circles are red light condition, n=20-32, 2way ANOVA and Bonferroni posttests, *p<0.05, **p<0.01. Scatter plot show mean +/- s.e.m. (**a**-**b**,**d**-**h**).

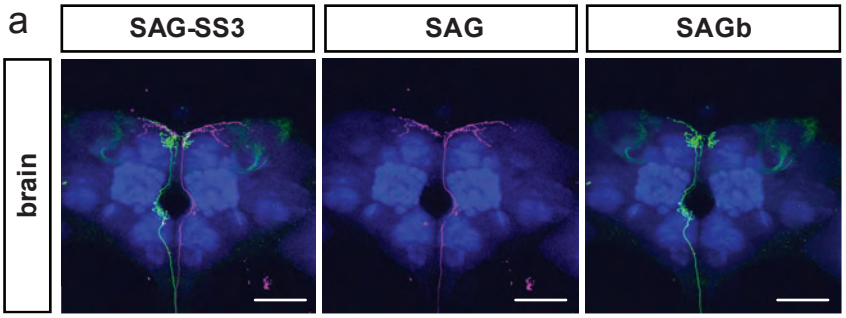
a
SAG-SS3
SAG
SAGb
brain

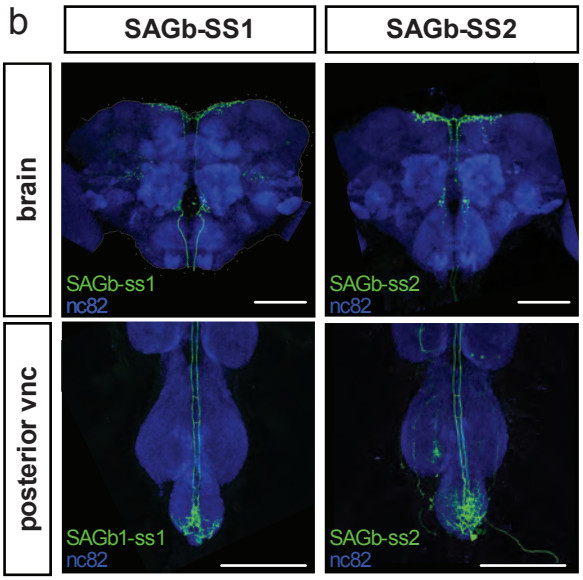
b
SAGb-SS1
SAGb-SS2
brain
SAGb-ss1
nc82
SAGb-ss2
nc82
posterior vnc
SAGb1-ss1
nc82
SAGb-ss2
nc82

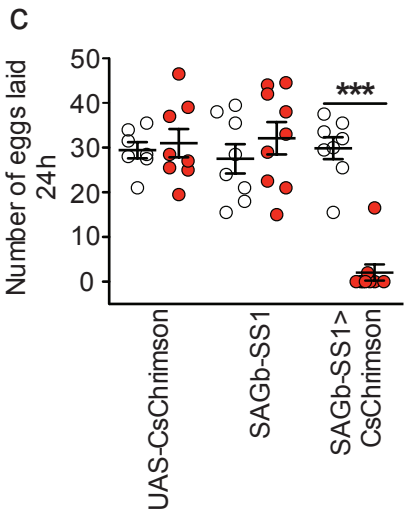
c
Number of eggs laid 24h
50
40
30
20
10
0
***
UAS-CsChrimson
SAGb-SS1
SAGb-SS1> CsChrimson

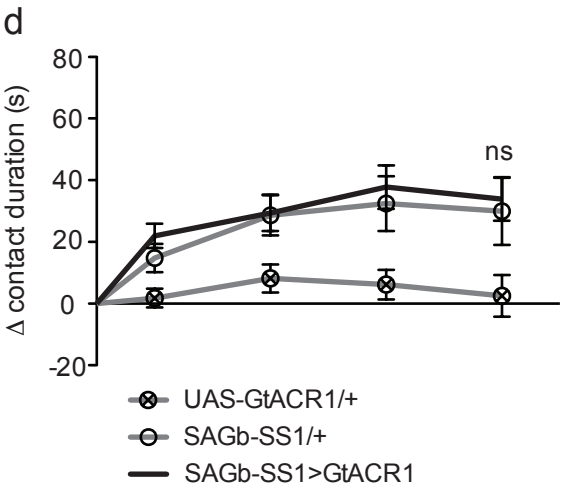
d
Δ contact duration (s)
80
60
40
20
0
-20
ns
UAS-GtACR1/+
SAGb-SS1/+
SAGb-SS1>GtACR1

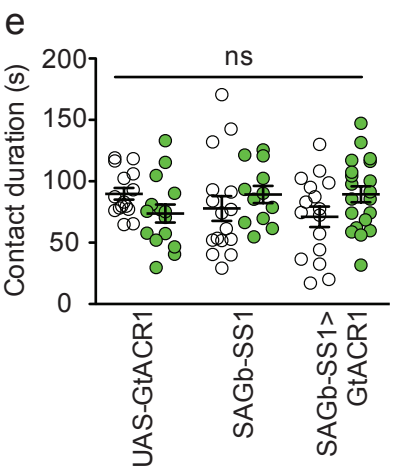
e
Contact duration (s)
200
150
100
50
0
ns
UAS-GtACR1
SAGb-SS1
SAGb-SS1> GtACR1

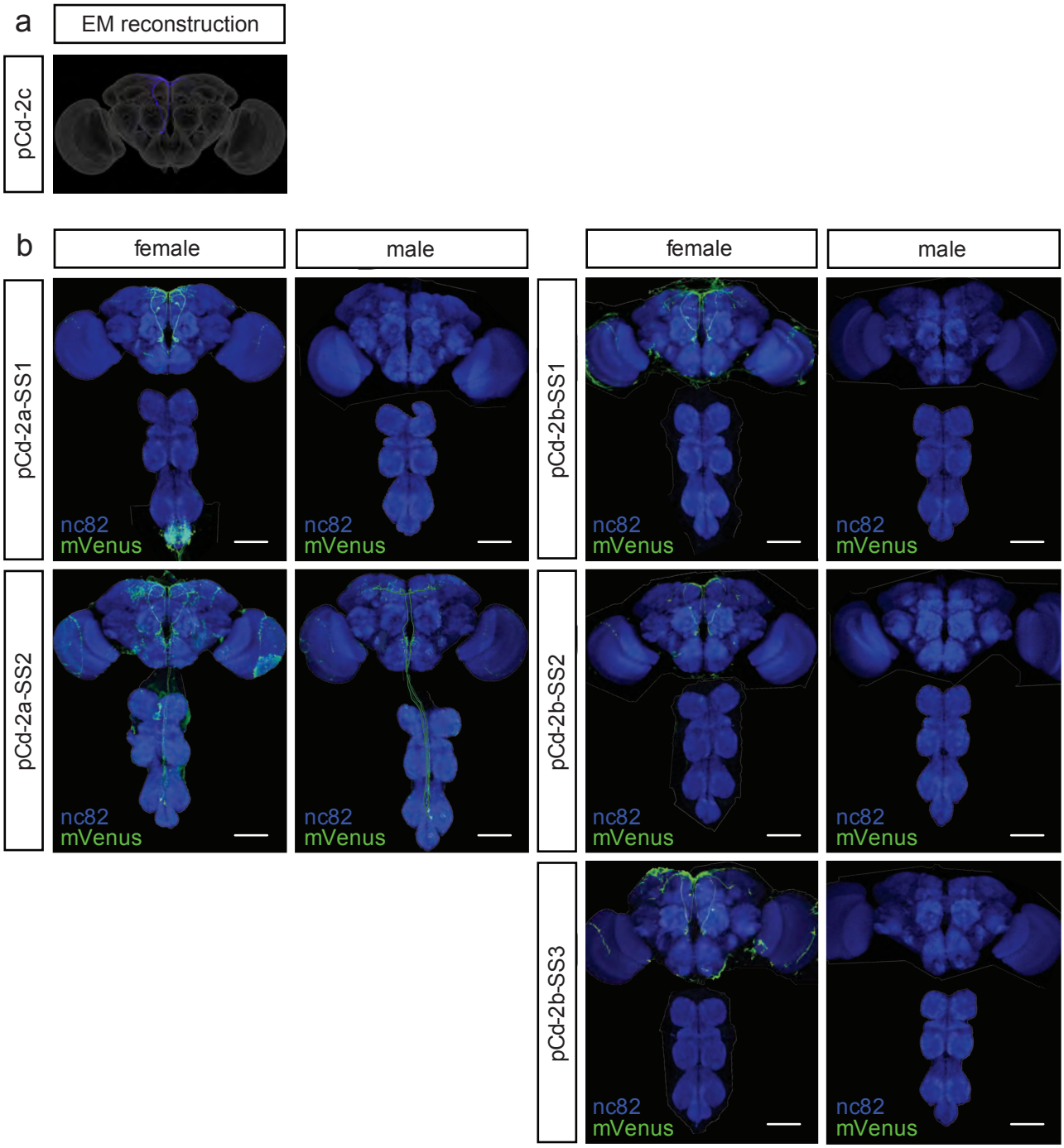
a
EM reconstruction
pCd-2c
b
female
male
female
male
pCd-2a-SS1
pCd-2b-SS1
pCd-2a-SS2
pCd-2b-SS2
pCd-2b-SS3
nc82
mVenus

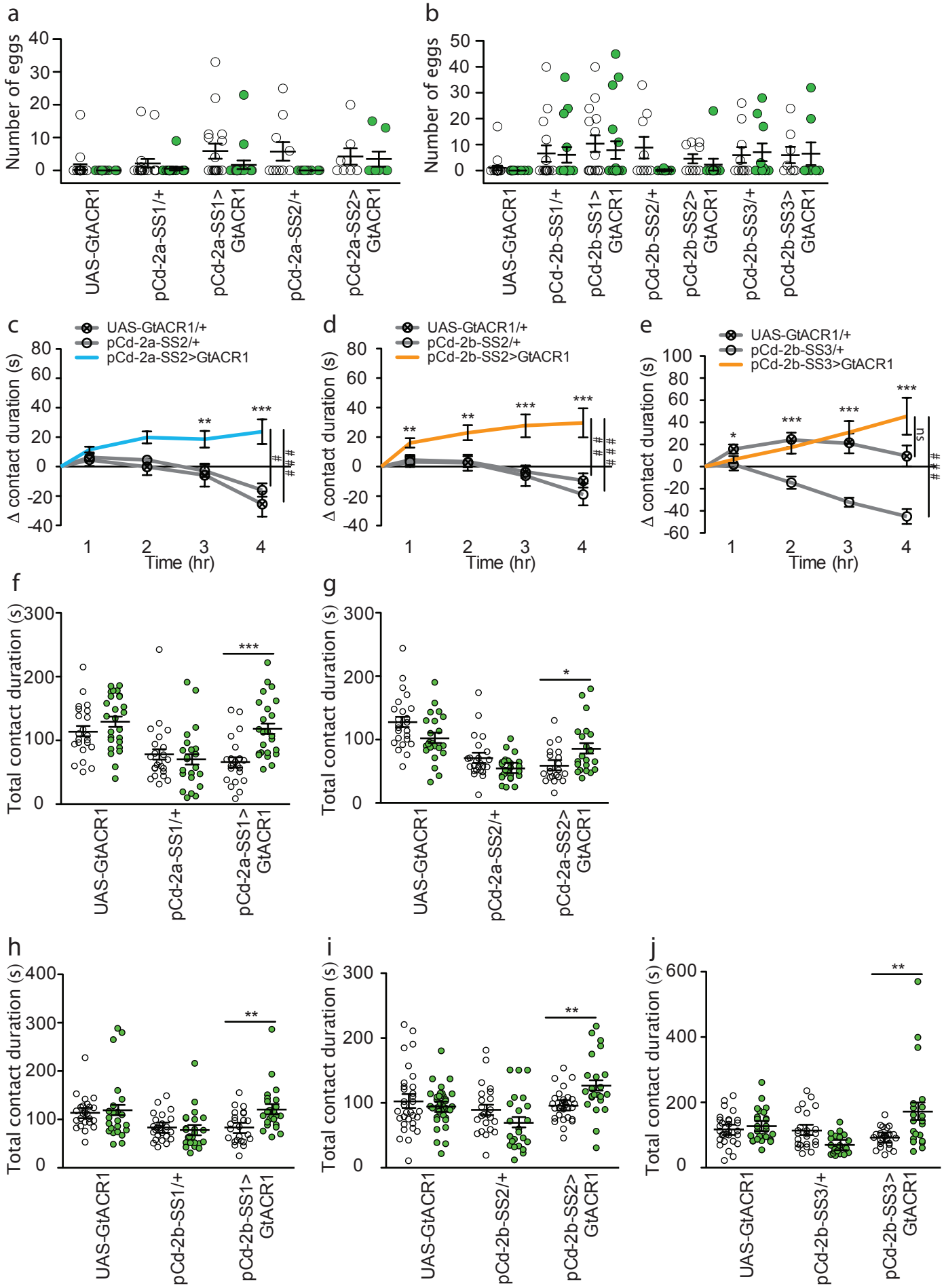
a
Number of eggs
UAS-GtACR1
pCd-2a-SS1/+
pCd-2a-SS1> GtACR1
pCd-2a-SS2/+
pCd-2a-SS2> GtACR1
b
Number of eggs
UAS-GtACR1
pCd-2b-SS1/+
pCd-2b-SS1> GtACR1
pCd-2b-SS2/+
pCd-2b-SS2> GtACR1
pCd-2b-SS3/+
pCd-2b-SS3> GtACR1
c
UAS-GtACR1/+
pCd-2a-SS2/+
pCd-2a-SS2>GtACR1
Δ contact duration (s)
Time (hr)
d
UAS-GtACR1/+
pCd-2b-SS2/+
pCd-2b-SS2>GtACR1
Δ contact duration (s)
Time (hr)
e
UAS-GtACR1/+
pCd-2b-SS3/+
pCd-2b-SS3>GtACR1
Δ contact duration (s)
Time (hr)
ns
f
Total contact duration (s)
UAS-GtACR1
pCd-2a-SS1/+
pCd-2a-SS1> GtACR1
g
Total contact duration (s)
UAS-GtACR1
pCd-2a-SS2/+
pCd-2a-SS2> GtACR1
h
Total contact duration (s)
UAS-GtACR1
pCd-2b-SS1/+
pCd-2b-SS1> GtACR1
i
Total contact duration (s)
UAS-GtACR1
pCd-2b-SS2/+
pCd-2b-SS2> GtACR1
j
Total contact duration (s)
UAS-GtACR1
pCd-2b-SS3/+
pCd-2b-SS3> GtACR1

Extended Data Fig. 5. Independent pCd-2a and pCd-2b lines regulate postmated sucrose consumption.

a-**b**, Number of eggs laid in 24 hours by virgin females of indicated genotype while exposed to green light (green) or no light (white). 2way ANOVA analysis revealed no significant differences between groups (n=9-20). **c**-**e**, Drinking time of females exposed to light normalized to dark controls of indicated genotype in FLIC over 4-hrs (n=19-36), Kruskal-Wallis, Dunn's posthoc at hour 4, ###p<0.001. Line graph shows mean and s.e.m. over time. **f**-**j** Total drinking time in FLIC in 4-hr assay (n=20-24). Analyzed with a 2way ANOVA and Bonferroni posttests (n=19-36). *p<0.05, **p<0.01, ***p<0.001, ns = not significant. Scatter plot show mean +/- s.e.m. (**a**-**b**,**f**-**j**).

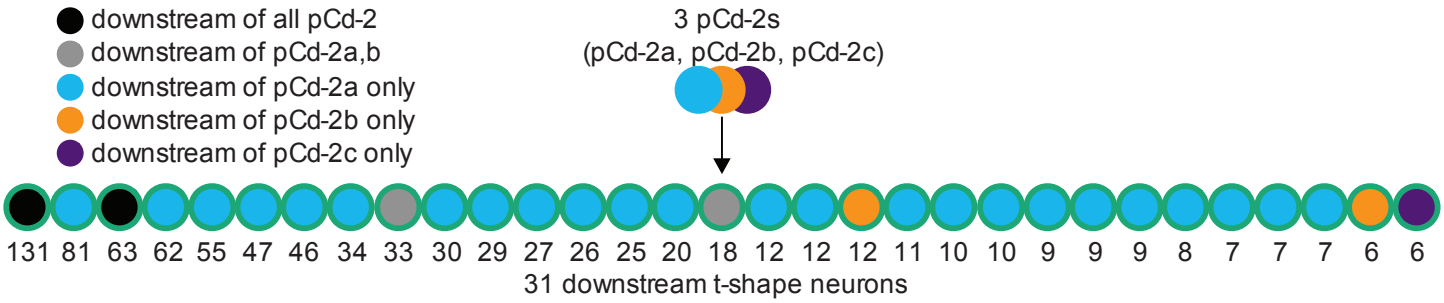

Fly Wire IDs from left to right
720575940613895934
720575940628750718
720575940628422555
720575940616987426
720575940610815510
720575940606550706
720575940620156513
720575940615716753
720575940632607127
720575940623115499
720575940628121143
720575940625126192
720575940632733792
720575940630247784
720575940618115669
720575940625960360
720575940632879842
720575940641886605
720575940634391950
720575940620201084
720575940616044834
720575940613988242
720575940627466746
720575940629491275
720575940620064321
720575940629944407
720575940615979067
720575940613234591
720575940622386056
720575940625850212
720575940613943714

Extended Data Fig. 6. Post-synapatic targets of pCd-2.
Schematic of neural connectivity of pCd-2 cells and downstream t-shape neurons identified by electron microscopy reconstruction. Number indicates number of synapses.

Methods

Rearing conditions and strains: Flies were reared on standard cornmeal-agar-molasses medium, at 25°C, 65% humidity on a 12-hr-light-dark cycle. Flies used in optogenetic assays were reared on food containing 0.25mM all-trans-retinal (Sigma-Aldrich) in darkness, before and after eclosion.
Flies were collected under CO_2 1-8h after eclosion and housed in same-sex groups. To generate mated females, 15 virgin females and 5 males were paired 3-5 days post-eclosion and group housed for 72 hours. To generate recently mated females, a single virgin female was paired with a single male for 2 hours. If mating was observed, the recently mated female was then immediately placed into indicated assay. To generate 24-hr mated females, a single virgin female was paired with a single male for 2 hours. If mating was observed, the recently mated female was then group housed with other recently mated females until testing. To generate egg-less females we used either ovoD mutant females[23] or hsp70-bam females[22] following the heat-shock protocol[7].

Capillary feeding (CAFE) assay: Capillary feeding arenas were modified from the original[20]. Briefly, we equipped a plastic vial, containing a wet kimwipe, with an altered rubber stopper lid housing two truncated 200-ml pipette tips whereby the capillaries can be inserted through. The capillaries (calibrated glass micropipettes, 5 ml) were loaded with 50mM sucrose solution containing 0.25 mg/ml blue dye. To measure sucrose consumption, 5 virgin or mated females were gently aspirated into an arena for 24 hours, the displacement of the meniscus was measured, and the volume per fly was calculated (1mm = 0.038ml).

Fly liquid interaction counter (FLIC): Females of indicated genotype or mating status were first wet-starved for 12-18 hours. Following this, females were then gently aspirated into the fly liquid food interaction counter (FLIC[18]), which was pre-filled with sucrose solution of indicated concentration. The voltage from each well was continuously recorded and a .csv file was produced. Significant changes in the voltage indicated that the fly was contacting the liquid. Contact duration acted as a proxy for consumption time. Based on a video analysis of flies drinking in FLIC in our lab, we modified the parameters in R to better model consumption. The new parameters are as follows: Feeding.Interval.Minimum = 10, Feeding.Threshold.Value = 10, Tasting.Threshold.Interval = c(01,02), Feeding.Minevents = 6, Signal.Threshold = 10.
For optogenetic control of neural activity prior to FLIC, we placed vials containing flies into a custom made light box (20cm x 10cm x 30cm) equipped with a string of 150 LED lights programmed with an Arduino to have green light constantly on.
For optogenetic control of neural activity while flies were in the FLIC, we designed and constructed a 12-chamber lid equipped with either 3 red LEDs (617nm, Luxeon Star, catalog number SP-01-E6) or 3 green LEDs (530nm, Luxeon Star, catalog number SP-01-G4). The 12-chamber cover was made from half of a 24-well plate, which was trimmed to fit. Lights were attached onto half of the 24-well plate lid and fitted atop the chamber cover.

Proboscis extension response (PER) assay: Females of indicated mating status were either wet-starved for 12-18 hours (starved) or kept on standard food (fed). Flies were then anesthetized using CO_2 and fixed to a glass slide with No More Nails polish and then allowed to recover for 2 hours in a humidified box. Immediately before testing, flies were given water until they no

345 longer responded to 5 consecutive presentations. Flies were then presented 3 times with sucrose
346 of an indicated concentration and proboscis extension was recorded.
347
348 **Temporal consumption assay (TCA):** Flies were starved for 18 hours in darkness, anesthetized
349 using CO_2 and then fixed to a glass slide with No More Nails polish with limited light and
350 allowed to recover for 2 hours in a humidified red light LED box or a humidified dark box.
351 Immediately before testing, flies were given water until they no longer responded to 5
352 consecutive presentations. In testing, flies were presented with 250 mM sucrose and
353 consumption time was recorded. Each trial ended when the fly was presented with the tastant and
354 no longer responded to 5 consecutive presentations. Flies in the dark condition were given water
355 and tested in low light conditions. Flies in red light condition were given water and tested in the
356 presence of red light.
357
358 **Egg laying assay:** 7-day old females were placed in a vial with standard food and placed into a
359 custom-made light box (20cm x 10cm x 30cm) that was equipped with a string of 150 LED
360 lights programmed with an Arduino. In neural activation tests, red light was transiently on (1
361 second on/1 second off). In neural silencing tests, green light was constantly on. Half of the
362 females of each genotype were placed in vials wrapped in foil to function as no-light condition
363 controls. After 24 hours, females were removed and eggs were immediately counted.
364
365 **Locomotor assay:** Locomotor assays were conducted as described[39].
366
367 **In vivo calcium imaging with taste stimulation:** Protocol was adapted[31]. Virgin and mated
368 females aged 14-20 days and mated females were co-housed with Canton-S males. Females were
369 food-deprived for 18-24 hours prior to imaging. A window was made in the head of the fly to
370 allow for visualization of the SEZ and a drop of ~250 mOsmo AHL solution
371 (https://www.sciencedirect.com/science/article/pii/S0092867403000047) was added to the head
372 and imaging was immediately performed on a fixed-stage 3i spinning disk confocal microscope
373 with a piezo drive and a 20x water objective (1.6x optical zoom). A 250 mM sucrose solution
374 was delivered to the proboscis using a glass capillary. To analyze these images, a maximum
375 intensity projection encompassing the arbors of Gr64f neurons was made using Fiji. Large ROIs
376 were drawn manually corresponding to the GCaMP expression and a large ROI was drawn in an
377 adjacent region to measure background autofluorescence. Mean fluorescence levels from the
378 background ROI were subtracted from the Gr64f ROIs at each time point, resulting in the
379 fluorescence trace over time: F(t). delta F/F was measured as follows: (F(t) – F(0)) / F(0), where
380 F(0) was the average of 10 time points before stimulation with sucrose and F(t) was the average
381 background subtracted increases in fluorescence during sucrose stimulation. Area under the
382 curve for 10 frames before stimulation and during stimulation was approximated with the
383 trapezoidal rule in Python using the NumPy.trapz function. Statistical analysis was carried out in
384 Python using the SciPy package, version 1.7.3 (https://www.nature.com/articles/s41592-019-
385 0686-2). deltaF/F0 images were created as described[40].
386
387 **In vivo functional connectivity experiments**: In vivo sample preparation for calcium imaging
388 was performed as described[31]. Prior to imaging, female flies were aged for 2 weeks and then
389 food-deprived in a vial containing a distilled water-soaked kimwipe for 18–24 hours prior to
390 imaging. Female flies were housed with Canton-S males throughout aging and food-deprivation.

391 Following dissection, samples were bathed in ~250 mOsmo AHL solution
392 (https://www.sciencedirect.com/science/article/pii/S0092867403000047) and imaged
393 immediately using a 2-photon microscope. Volumetric images of the prow region were acquired
394 with 920 nm light at 2.9 Hz with resonant scanning and a piezo-driven objective. During
395 imaging, a custom ScanImage plugin was used to deliver two 10-second pulses of 660 nm light
396 through the objective at a 10-second interval to excite CsChrimson.
397 Image and statistical analysis of functional connectivity experiments was performed using Fiji
398 (https://www.nature.com/articles/nmeth.2019), CircuitCatcher (a customized python program by
399 Daniel Bushey), and Python (Python Software Foundation, https://www.python.org/). Using Fiji,
400 image stacks for each time point were first maximum intensity projected. Then, using
401 CircuitCatcher, an ROI containing Lrg3+ mBN cell bodies and a background ROI of brain tissue
402 were selected and the average fluorescence intensity for each ROI at each timepoint was
403 retrieved. Then, in Python, background subtraction was carried out for each timepoint (F_t) and
404 initial fluorescence intensity ($F_{initial}$) was calculated as the mean corrected average fluorescence
405 intensity for frames 1-15. Then, $\Delta F/F$ was calculated using the following formula: F_t-$F_{initial}/F_{initial}$.
406 Area under the curve for before (off; frames 1-29) and during (on; frames 30-58) light
407 stimulation was approximated with the trapezoidal rule in Python using the NumPy.trapz
408 function. Statistical analysis of functional connectivity experiments was carried out in Python
409 using the SciPy package, version 1.7.3 (https://www.nature.com/articles/s41592-019-0686-2).
410
411 **Dissections and Immunohistochemistry:** All CNS dissections and immunostaining (unless
412 directly addressed) were performed following the detailed instructions found at
413 https://www.janelia.org/project-team/flylight/protocols. To image split-GAL4 lines and
414 intersections, we used the following primary antibodies: mouse α-Brp (nc82, DSHB, University
415 of Iowa, USA) at 1:40, chicken α-GFP (Invitrogen, A10262) at 1:1000; and the following
416 secondary antibodies: goat α-mouse AF647 (Invitrogen, A21236) at 1:500, goat α-chicken
417 AF488 (Life Technologies, A11039) at 1:500. Multi-Color Flip-Out fly generation was
418 performed following the protocol[41]. For imaging, we used the following primary antibodies:
419 mouse α-Brp (nc82, DSHB, Univerisity of Iowa, USA) at 1:40, rabbit α-HA (rabbit α-HA (Cell
420 Signaling Technology, C29F4) at 1:1000, rat α-Flag (Novus Biologicals, NBP1-06712) at
421 1:1000; and the following secondary antibodies: goat α-mouse AF647 (Invitrogen, A21236) at
422 1:500, goat α-rabbit AF488 (Invitrogen, A11034) at 1:500, and goat α-rat AF568 (Invitrogen,
423 A11077) at 1:500.
424 Reproductive tract dissections and staining was performed as described[42]. As the primary
425 antibody, we used chicken α-GFP (Invitrogen, A10262) at 1:1000 followed by goat α-chicken
426 AF488 (Life Technologies, A11039) at 1:500 with the addition of Alexa Fluor 633 phalloidin
427 (ThermoFisher Scientific) to visualize the muscle-lined reproductive tract (1:500).
428
429 **Confocal imaging:** Samples were imaged on a LSM710 confocal microscope (Zeiss) with a
430 Plan-Apochromate 20x0.8 M27 objective and images were prepared in Fiji.
431
432 **Electron Microscopy neural reconstructions and connectivity:** SAG was previously partially
433 reconstructed[16] in the Full Adult Female Brain (FAFB[27]) electron microscopy dataset using the
434 CATMAID software[43]. We completed additional tracing of this neuron by continuing branches
435 with a combination of both manual and assisted tracing. Manual tracing consisted of generating a
436 skeleton of the neuron by following the neuron and marking the center of each branch. Assisted

437 tracing consisted of joining and proofreading pre-assembled skeleton fragments with automated
438 segmentation[44]. In addition to the skeleton tracing, new chemical synapses were also annotated
439 as previously described[27]. Finally, downstream synaptic targets of SAG were then traced out
440 from these additional locations using both manual and assisted tracing techniques as described
441 above.
442 Neurons traced in CATMAID, including SAG, pC1, egg-laying circuit neurons[16] and sexual
443 receptivity circuit neurons[17], were all located in Flywire (flywire.ai), which uses the same EM
444 electron microscopy dataset[27]. To identify synaptic partners, we used connectome annotation
445 versioning engine (CAVE[25,26]) using a cleft score cutoff of 100 to generate synapses of relatively
446 high confidence[26].
447
448 **Intersectional method to access SPSNs:**
449 Based on previous reports, three genetic drivers label the SPSN (VT003280[3], fru[14,15] and
450 ppk[14,15]) with driver lines available in two separate binary expression systems (UAS-GAL4
451 and LexA-LexAop). With the use of a conditional reporter line (UAS < stop < GFP) and in
452 combination with inducible FLP line (LexAopFLP) three combinations were produced: fru-
453 LexA∩ppk-GAL4, fru-LexA∩VT3280-GAL4, and VT3280-LexA∩ppk-GAL4. Images of the
454 female reproductive tract were used to confirm labeling of the SPSNs and images of the brain to
455 determine off-target neural expression. With the use of a conditional effector line (UAS < stop <
456 KIR or UAS < stop < TNT), SPSNs were silenced and females (along with genetic controls)
457 were tested for changes in sucrose consumption.
458
459 **Split-GAL4 screening and stabilization**
460 pCd-2 split generation:
461 Using the FlyEM Hemibrain V1.2.1 dataset via NeuPRINT, we queried "SAG" and explored the
462 output neuron list, identifying three pCd-2 neurons per hemisphere (SMP286, SMP287,
463 SMP288). From here, we used Neuron Bridge to manually explore the light microscopy matches
464 and generated a list of possible hemi-driver that labeled this cell type. The expression pattern of
465 the p65ADZp and ZpGAL4DBD combinations were examined by driving the expression of UAS
466 reporter (20xUAS-CsChrimson-mVenus in attP18). Combinations with specific expression in
467 pCd-2 neurons were stabilized.
468
469 SAGb split generation:
470 Using Neuron Bridge, we queried "VT050405" (the genetic construct used as the p65ADZp
471 hemidriver in SAG-SS3) and identified multiple "Body Ids" that morphologically matched the
472 non-SAG ascending cell type. From here we generated a "Color Depth Search" to create a list of
473 possible hemi-driver that labeled this cell type. The expression pattern of the p65ADZp and
474 ZpGAL4DBD combinations were examined by driving the expression of UAS reporter
475 (20xUAS-CsChrimson-mVenus in attP18) and combinations with specific expression in SAGb
476 neurons were stabilized.
477
478 **Statistical analysis:** Statistical tests for all experiments, with the exception of in vivo calcium
479 imaging and in vivo functional connectivity experiments, were performed in GraphPad Prism.
480 For two- and three-group comparisons, data was first tested for normality with the KS normality
481 test (alpha = 0.05). If all groups passed then groups would be compared with a parametric test (t-
482 test or One-Way ANOVA, respectively). If at least one group did not pass, groups were

compared with a non-parametric version (Mann-Whitney test or Kruskal-Wallis test, respectively). For all multi-factorial designs, a Two-Way ANOVA was performed with a Bonferroni post-hoc test. All statistical tests, significance levels, and number of data points (N) are specified in the figure legend.

Normalized data sets: Most datasets from optogenetic assays were normalized within each genotype. To generate this normalized dataset, data from females within the no light condition was averaged, creating a "no-light mean" for each genotype. This value was subtracted from each individual female within the light condition of the corresponding genotype. This dataset was then graphed and statistical analysis was performed as outlined above.

39. Bidaye, S. S., Laturney, M., Chang, A. K., Liu, Y., Bockemühl, T., Büschges, A. & Scott, K. Two brain pathways initiate distinct forward walking programs in Drosophila. *Neuron***108**, doi: 10.1016/j.neuron.2020.07.032 (2020).
40. Yao, Z. & Scott, K. Serotonergic neurons translate taste detection into internal nutrient regulation. *Neuron***110**, 1036-1050 (2022).
41. Nern, A., Pfeiffer, B. D. & Rubin, G. M. Optimized tools for multicolor stochastic labeling reveal diverse stereotyped cell arrangement in the fly visual system. *Proc. Natl. Acad. Sci. USA***112**, E2967-2976 (2015)
42. Billeter, J. C. & Goodwin, S. F. Characterization of Drosophila fruitless-gal4 transgenes reveals expression in male-specific fruitless neurons and innervation of male reproductive structures. *J. Comp. Neurol*. **475**, 270-287 (2004).
43. Saalfeld, S., Cardona, A., Hartenstein, V. & Tomancak, P. CATMAID: collaborative annotation toolkit for massive amounts of image data. *Bioinformatics***25**, 1984-1986 (2009).
44. Li, F., Lindsey, L. F., Januszewski, M., Tyka, M., Maitin-Shepard, J., Blakely, T. & Jain, V. Automated reconstruction of a serial-section EM Drosophila brain with flood-filling networks and local realignment. *Micro. Microanal*. **25**, 1364-1365 (2019).

Figure	short genotype	full genotype
1n-o	Gr65f-GAL4 > GCaMP	*UAS-CD8::tdTomato/+;20xUAS-IVS-GCaMP6s(attP40)/Gr64f-GAL4; 20xUAS-IVS-GCaMP6s(VK00005)/Gr64f-GAL4*
2a	hs-bam	*Hsp70(generic)-bam.O;+;+*
2c	fru-LexA ∩ ppk-GAL4 > GFP	*w*; 8xLexAop2-FLPL(attP40)/UAS(FRT.stop)Hsap\mcd8::GFP(VIE-19a); Fru-PI-LexA/ppk-GAL4*
2d	fru-LexA ∩ ppk-GAL4 > TNT	*w+; 8xLexAop2-FLPL(attP40)/w[+m*]=UAS(FRT.stop)Ctet\tetX(VIE-19A); Fru-PI-LexA/ppk-GAL4*
2d	fru-LexA, UAS-TNT (control)	*w+; w[+m*]=UAS(FRT.stop)Ctet\tetX(VIE-19A)/+; Fru-PI-LexA/+*
2e	fru-LexA ∩ ppk-GAL4 > KIR2.1	*w+;8xLexAop2-FLPL(attP40)/UAS(FRT.stop)Hsap\KCNJ2(VIE-19A); Fru-PI-LexA/ppk-GAL4*
2e	fru-LexA, UAS-KIR (control)	*w+; UAS(FRT.stop)Hsap\KCNJ2(VIE-19A)/+; Fru-PI-LexA/+*
2d,e	ppk-GAL4 (control)	*w+;8xLexAop2-FLPL(attP40)/+;ppk-GAL4/+*
2f	SAG-SS3 > GFP	*w*;20xUAS-csChrimson::mVenus(attP18)/+; VT050405-p65.AD(attP40)/+;dsx^{DBD}/+*
2g	SAG-SS3 > GtACR1	*w+; VT050405-p65.AD(attP40)/+;20xUAS-IVS-GtACR1 EYFP(attP2)/dsx^{DBD}*
2g	SAG-SS3 (control)	*w+; VT050405-p65.AD(attP40)/+; dsx^{DBD}/+*
2h	pC1-SS1 > GFP	*w*;20xUAS-csChrimson::mVenus(attP18)/+; VT002064-p65AD(attP40)/+; VT008469-GAL4DBD(attP2)/+*
2i	pC1-SS1 > GtACR1	*w+; VT002064-p65AD(attP40)/+;20xUAS-IVS-GtACR1-EYFP(attP2)/VT008469-GAL4DBD(attP2)*
2i	pC1-SS1 (control)	*w+; VT002064-p65AD(attP40)/+; VT008469-GAL4DBD(attP2)/+*
2g,i	GtACR1 (control)	*w+; +; 20xUAS-IVS-GtACR1-EYFP(attP2)/+*
3b	vpoDN-SS1 > GtACR1	*w+; 31D07-p65AD(attP40)/+;20xUAS-IVS-GtACR1 EYFP(attP252F12-GAL4DBD(attP2)*
3b	vpoDN-SS1 (control)	*w+; 31D07-p65AD(attP40)/+;52F12-GAL4DBD(attP2)/+*
3c	vpoDN-SS2 > GtACR1	*w+; VT045670-p65AD(attP40)/+; 20xUAS-IVS-GtACR1-EYFP(attP2)/52F12-GAL4DBD(attP2)*
3c	vpoDN-SS2 (control)	*w+; VT045670-p65AD(attP40)/+;52F12-GAL4DBD(attP2)/+*
3b,c	GtACR1 (control)	*w+; +; 20xUAS-IVS-GtACR1-EYFP(attP2)/+*
3d-f	oviDN-SS1 > csChrimson	*w*,20xUAS-csChrimson::mVenus(attP18)/+; VT050660-p65.AD(attP40)/+; VT028160-GAL4DBD(attP2)/+*
3d-f	oviDN-SS1 (control)	*w*; VT050660-p65.AD(attP40)/+; VT028160-GAL4DBD(attP2)/+*
3d-g	csChrimson (control)	*w*,20xUAS-csChrimson::mVenus(attP18)/+;+*
3d,e,g	oviDN-SS2 > csChrimson	*w*,20xUAS-csChrimson::mVenus(attP18)/+; VT026873-p65.AD (attP40)/+; VT040574-GAL4DBD(attP2)/+*
3d,e,g	oviDN-SS2 (control)	*w*; VT026873-p65.AD(attP40)/+; VT040574-GAL4DBD(attP2)/+*
4e	pCd-2a-SS1 > GFP	*w*,20xUAS-csChrimson::mVenus(attP18)/+; VT027804-p65.AD(attP40)/+; dsx^{DBD}/+*
4f	pCd-2b-SS1 > GFP	*w*,20xUAS-csChrimson::mVenus(attP18)/+; R9B05-p65.AD(attP40)/+; R22D06-GAL4DBD(attP2)/+*
4g,h	pCd-2a-SS1 > GtACR1	*w+; VT027804-p65AD(attP40)/20xUAS-IVS-GtACR1-EYFP(attP2)/dsx^{DBD}*
4g,h	pCd-2a-SS1 (control)	*w+; VT027804-p65AD(attP40)/+; dsx^{DBD}/+*
4g,i	pCd-2b-SS1 > GtACR1	*w+; R9B05-p65AD(attP40)/20xUAS-IVS-GtACR1-EYFP(attP2)/R22D06-GAL4DBD(attP2)/+*
4g,I	pCd-2b-SS1 (control)	*w+; R9B05-p65AD(attP40)/+; R22D06-GAL4DBD(attP2)/+*
4g-I	GtACR1 (control)	*w+; +; 20xUAS-IVS-GtACR1-EYFP(attP2)/+*
5d	pC1-SS1 > Chrimson, Lgr3 > GCaMP6s	*w*,LexAop2-syn21-opGCaMP6s,10x-UAS-syn21-Chrimson88-tdTomato; VT002064-p65AD(attP40)/R19B09-LexA(attp40); VT008469-GAL4DBD(attP2)/+*
5e	pCd-2a-SS1 > Chrimson, Lgr3 > GCaMP6s	*w*,LexAop2-syn21-opGCaMP6s,10x-UAS-syn21-Chrimson88-tdTomato; VT027804-p65AD(attP40)/R19B09-LexA(attp40);*

		dsx^{DBD}/+
5f	pCd-2b-SS1 > Chrimson, Lgr3 > GCaMP6s	*w*,LexAop2-syn21-opGCaMP6s,10x-UAS-syn21-Chrimson88-tdTomato; R9B05-p65AD(attP40)/R19B09-LexA(attp40); R22D06-GAL4DBD(attP2)/+*
5d-f	control	*w*,LexAop2-syn21-opGCaMP6s,10x-UAS-syn21-Chrimson88-tdTomato; R19B09-LexA(attp40)/+;+*
5h	Lgr3 ∩ Fru > csChrimson	*w-,20xUAS(FRT.stop)csChrimson:mVenus(attP18)/+; 8xLexAop2-FLPL(attP40)/+; Fru-PI-LexA/R19B09-GAL4*

Supplementary Table 1 | Fly genotypes in figures

Type	Name	Genotype	Reference/Source
Wild-type	Canton-S	w+;+;+	N/A
Driver	Gr64f-Gal4	w-;Gr64-gal4;+	RRID: BDSC_57669
Driver	Gr64f-Gal4	w-;+;Gr64f-gal4	RRID: BDSC_57668
Reporter	UAS-GCaMP	w-;UAS-GCaMP6s(attP40);+	RRID: BDSC_42746
Reporter	UAS-GCaMP	w-;+;UAS-GCaMP6s(VK00005)	RRID: BDSC_42749
Reporter	UAS-tdTomato	UAS-CD8-tdTomato;+;+	[45]
Effector	ovoD	w+;+;ovoD1	[23]
Effector	hs-BAM	hs-bam,w1118;+;+	RRID: BDSC_24636
Driver	nsyb-Gal4	w-;+;nsyb-gal4	RRID: BDSC_51941
Effector	UAS-dcr2	w-;UAS-dcr-2;+	RRID: BDSC_24650
Effector	UAS-SPR-RNAi	w-;+;UAS-SPR-IR1	[13]
Driver	Ppk-gal4	w-;+;ppk-gal4	RRID: BDSC_32079
Driver	VT3280-Gal4	w-;+;VT003280-gal4 attP2	[3]
Driver	VT3280-LexA	w-;+;VT003280-LexA attP2	[3]
Driver	Fru-LexA	w-;+;$Fru^{P1\text{-}LexA}$	[46]
Effector	LexAop2-FLPL	w-;8xLexAop2-FLPL(attP40);+	RRID: BDSC_55820
Effector	UAS>stop>KIR	w+;UAS > stop > KIR	RRID: BDSC_67686
Effector	UAS>stop>TNT	w+;UAS > stop > TNT	RRID: BDSC_67690
Reporter	UAS>stop>GFP	w-;UAS > stop > CD8::GFP;+	RRID: BDSC_30125
Driver	SAG-SS3	VT050405-p65ADZp(attP40);	[47]
		dsx-ZpGal4DBD	[48]
Driver	pC1-SS1	VT002064-p65ADZp(attP40);	[16]
		VT008469-ZpGal4DBD(attP2)	
Driver	pC1-SS2	VT002064-p65ADZp(attP40);	[16] (modified)
		dsx-ZpGal4DBD	
Driver	vpoDN-SS1	31D07-p65ADZp(attP40);	[17]
		52F12-ZpGal4DBD(attP2)	
Driver	vpoDN-SS2	VT045670-p65ADZp(attP40);	[17]
		52F12-ZpGal4DBD(attP2)	
Driver	oviIN-SS1	68A10-p65ADZp(attP40);	[16]
		VT010054-ZpGal4DBD(attP2)	
Driver	oviIN-SS2	VT026347-p65ADZp(attP40);	[16]
		VT026035-ZpGal4DBD(attP2)	
Driver	oviDN-SS1	VT050660-p65ADZp(attP40);	[16]
		VT028160-ZpGal4DBD(attP2)	
Driver	oviDN-SS2	VT026873-p65ADZp(attP40);	[16]
		VT040574-ZpGal4DBD(attP2)	
Effector	UAS-GtACR	w+;;20xUAS-IVS-GtACR1-EYFP9attP2)	[49]
Effector	UAS-csChrimson,	w-,20xUAS-ssChrimson::mVenus(attP18);+;+	RRID: BDSC_55134
Effector	MCFO		RRID: BDSC_
Driver	SAGb-SS1	VT004974-p65ADZp(attP40);	RRID: BDSC_71475
		R69H11-ZpGal4DBD(attP2)	RRID: BDSC_69819
Driver	SAGb-SS2	VT023823-p65ADZp(attP40);	[47]
		R69H11-ZpGal4DBD(attP2)	RRID: BDSC_69819
Driver	pCd-2a-SS1	VT027804-p65ADZp(attP40);	RRID: BDSC_72041
		dsx-ZpGal4DBD	[48]
Driver	pCd-2a-SS2	VT057275-p65ADZp(attP40);	RRID: BDSC_71664
		VT027804-ZpGal4DBD(attP2)	RRID: BDSC_71758
Driver	pCd-2b-SS1	R9B05-p65ADZp(attP40);	RRID: BDSC_70519
		R22D06-ZpGal4DBD(attP2)	[50]
Driver	pCd-2b-SS2	R29G03-p65ADZp(attP40);	RRID: BDSC_75746
		R22D06-ZpGal4DBD(attP2)	[50]
Driver	pCd-2b-SS3	R60C09-p65ADZp(attP40);	RRID: BDSC_69750
		R22D06-ZpGal4DBD(attP2)	[50]

Driver	R19B09-gal4	R19B09-Gal4(attP2)	RRID: BDSC_48840
Driver	R19B09-LexA	R19B09-LexA(attP40)	RRID: BDSC_52539
Effector	UAS>stop>csChrimson w-	,UAS > stop > csChrimson(attP18)	[51]
Effector	UAS-Chrimson88	UAS-Chrimson88;+;+	[52]
Reporter	LexAop-GCaMP6s	LexAop-GCaMP6s;+;+	[53]

Supplementary Table 2 | Fly Stocks

Supplementary References

45. Thistle, R., Cameron, P., Ghorayshi, A., Dennison, L. & Scott, K. Contact chemoreceptors mediate male-male repulsion and male-female attraction during Drosophila courtship. *Cell***149**, 1140-1151 (2012).
46. Mellert, D. J., Knapp, J. M., Manoli, D. S., Meissner, G. W. & Baker, B. S. Midline crossing by gustatory receptor neuron axons is regulated by fruitless, doublesex and theh Roundabout receptors. *Development***137**, 323-332 (2010).
47. Tirian, L. & Dickson, B. J. The VT GAL4, LexA, and split-GAL4 driver line collections for targeted expression in the Drosophila nervous system. bioRxiv doi: https://doi.org/10.1101/198648.
48. Shirangi, T. R., Wong, A. M., Truman, J. W. & Stern, D. L. Doublesex regulates the connectivity of a neural circuit controlling Drosophila male courtship song. *Dev. Cell***37**, 533-544 (2016).
49. Mohammad, F., Stewart, J. C., Ott, S., Chlebikova, K., Chua, J. Y., Koh, T. W., Ho, J & Claridge-Chang, A. Optogenetic inhibition of behavior with anion channelrhodopsins. Nat. *Methods***14**, 271-274 (2017).
50. Dionne, H., Hibbard, K. L., Carvallaro, A., Kao, J. C. & Rubin, G. M. Genetic reagents for making split-GAL4 lines in Drosophila. *Genetics***209**, 31-35 (2018).
51. Wu, M., Nern, A., Williamson, W. R., Morimoto, M. M., Reiser, M. B., Card, G. M. & Rubin, G. M. Visual projection neurons in the Drosophila lobula link feature detection to distinct behavioral programs. *Elife*, doi: 10.7554/eLife.21022.
52. Klapoetke, N. C. et al. Independent optical excitation of distinct neural population. *Nature Methods***11**, 338-346 (2014).
53. Broussard, G. J. et al. In vivo measurement of afferent activity with axon-specific calcium imaging. *Nat. Neurosci*. **21**, 1272-1280 (2018).

Acknowledgements
Members of the Scott lab provided contributions to experimental design, data analysis, and manuscript preparation. Salil Bidaye assisted with the analyses of locomotor data. This work was supported by NIH R01DC013280 (K.S.). Neuronal reconstruction for this project took place in a collaborative CATMAID environment in which 27 labs are participating to build connectomes for specific circuits. Therefore, work done for published (Wang et al. 2020) and ongoing projects has proved useful to us. Development and administration of the FAFB tracing environment and analysis tools were funded in part by National Institutes of Health BRAIN Initiative grant 1RF1MH120679-01 to Davi Bock and Greg Jefferis, with software development effort and administrative support provided by Tom Kazimiers (Kazmos GmbH) and Eric Perlman (Yikes LLC). We thank Peter Li for sharing his automatic segmentation (citation is https://doi.org/10.1101/605634). Tracing in Cambridge was supported by Wellcome Trust (203261/Z/16/Z) and ERC (649111) awards to G. Jefferis. We thank the Princeton FlyWire team and members of the Murthy and Seung labs for development and maintenance of FlyWire (supported by BRAIN initiative grant MH117815 to Murthy and Seung). We found the partial tracing of SAG and pC1 in CATMAID useful (Wang et al. 2020). In addition to our tracing efforts, we are appreciative of the tracing accomplished by other labs. For help with tracing of pC1 in FlyWire, we thank the Murthy and Seung labs (77% of pC1a, 98% of pC1b, 92% of pC1c) and the Jefferis lab (7% of pC1a, 8% of pC1c). For help with tracing pCd-2 cells we would like to thank the Dickson lab (CATMAID: 76% of pCd-2a, 44% of pCd-2b, 28% of pCd-2c), the Jefferis lab (CATMAID: 20% of pCd-2a, 6% of pCd-2b, 3% of pCd-2c; FlyWire: 32% of pCd-2a, 8% of pCd-2b, 13% of pCd-2c), the Murthy and Seung lab (FlyWire: 15% of pCd-2a, 11% of pCd-2b, 6% of pCd-2c), and Janelia tracers (FlyWire: 52% of pCd-2a, 14% of pCd-2b). We would like to thank the Jefferis labs (46%) and the Murthy and Seung labs (50%) for their contribution to tracing the t-shaped Lgr3 cells. The tracers who contributed include Nora Forknall, Lily Talley, Katie Stevens, Shanice Bailey, Tansy Yang, Istvan Taisz, Greg Jefferis, Lucas Encarnacion-Rivera, Austin T. Burke, Yijie Yin, James Hebditch, Kyle Patrick Willie, Joshua Bañez, Philipp Schlegel, Dharini Sapkal, Irene Salgarella, Dhwani Patel, Ben Silverman, Bhargavi Parmar, Chitra Nair, Doug Bland, Laia Serratosa, Marta Costa, Nash Hadjerol, Regine Salem, Rey Adrian Candilada, Shirleyjoy Serona, Zairene Lenizo, Zeba Vohra, and Zepeng Yao.

Author contributions
M.L. and K.S. conceived and designed the study and wrote the manuscript. M.L. performed the experiments and analyzed the data with the exception of the functional imaging experiment, performed and analyzed by G.S.

Competing interests
The authors declare no competing interests.

Corresponence and requests for materials should be addressed to K.S. or M.L.